

Evidence for Low Universal Equilibrium Black Hole Spin in Luminous Magnetically Arrested Disks

BEVERLY LOWELL ¹, JONATAN JACQUEMIN-IDE ^{2,1}, MATTHEW LISKA ³ AND ALEXANDER TCHEKHOVSKOY ^{1,4}

¹Center for Interdisciplinary Exploration & Research in Astrophysics (CIERA), Physics and Astronomy, Northwestern University, Evanston, IL 60202, USA

²JILA, University of Colorado and National Institute of Standards and Technology, 440 UCB, Boulder, CO 80309-0440, USA

³Center for Relativistic Astrophysics, Georgia Institute of Technology, Howey Physics Bldg, 837 State St NW, Atlanta, GA, 30332, USA

⁴NSF-Simons AI Institute for the Sky (SkAI), 172 E. Chestnut St., Chicago, IL 60611, USA

ABSTRACT

Relativistic collimated outflows, or jets, provide a crucial mode of active galactic nucleus feedback. Although the jets extract their energy from the black hole (BH) rotation, their effect on the BH spin is poorly understood. Because the spin controls radiative and mechanical BH feedback, lack of first-principles models for BH spin evolution limits our ability to interpret observations, including the recent LIGO-Virgo-KAGRA spin constraints. Particularly important are luminous disks, which rapidly grow and strongly torque their BHs. Jet-less and weakly magnetized “standard” luminous disks *spin-up* their BHs to near-maximum dimensionless spin, $a_{\text{eq,NT}} = 0.998$. However, sufficient large-scale vertical magnetic flux can cause the inner disk to enter a magnetically arrested disk (MAD) state, whose jets can efficiently extract BH rotational energy and significantly *spin-down* the BH. Indeed, Lowell et al. (2024) found that non-radiative MADs *spin-down* their BHs to very low $a_{\text{eq,MAD}}^{\text{nr}} = 0.07$. Moreover, their analytic model predicted that luminous MADs also *spin-down* their BHs to low $a_{\text{eq,MAD}}^{\text{lum}} \sim 0.3 - 0.5$. To test this prediction, we perform 3D general relativistic (radiation) magnetohydrodynamic (GR(R)MHD) simulations of MADs across a wide range of BH spin ($-0.9 \leq a \leq 0.99$) and disk dimensionless thickness ($0.03 \leq h/r \leq 0.3$, which corresponds to Eddington ratio, $0.35 \leq \dot{m}/\dot{m}_{\text{Edd}} \leq \infty$). We find that luminous MADs *spin-down* their BHs to a low *universal* equilibrium spin value, $a_{\text{eq,MAD}}^{\text{lum}} \approx 0.3$ for $0.03 \leq h/r \leq 0.1$. Moreover, we find evidence for quadratic convergence, $a_{\text{eq,MAD}} \approx 0.31 - 2.71(h/r)^2 \rightarrow 0.31$ as $h/r \rightarrow 0$. We attribute this to disk thermodynamics becoming irrelevant as the cooling becomes more aggressive and magnetic forces start to dominate. We finish by discussing the astrophysical implications.

Keywords: Black holes — relativistic jets — black hole spin – magnetohydrodynamics

1. INTRODUCTION

Relativistic jets are observed across a range of astrophysical objects, including active galactic nuclei (AGN), ranging from low luminosity AGN (e.g., M87) to luminous quasars (Kong & Ho 2018), X-ray binaries (XRBs, Done et al. 2007), tidal disruption events (TDEs, Burrows et al. 2011; Bloom et al. 2011; Tchekhovskoy et al. 2014), and gamma ray bursts (GRBs) powered by collapsars (Woosley 1993; Goldstein et al. 2016) and neutron star (NS) mergers (Foucart et al. 2015; Metzger 2019; Nakar 2020).

A popular mechanism for jet launching is the Blandford-Znajek (BZ) mechanism (Blandford & Znajek 1977). In this mechanism, large-scale magnetic flux taps into the spin energy of the black hole (BH) and leads to BH spin-down. The

jet power scales approximately as $P_{\text{jet}} \sim \Phi_{\text{BH}}^2 a^2$, where Φ_{BH} is the magnetic flux on the BH, and $-1 \leq a \leq 1$ is the dimensionless BH spin (Blandford & Znajek 1977; Komissarov 1999; Tchekhovskoy et al. 2010).

Since BH spin controls jet power, it is crucial to understand what determines the spin across different astrophysical sources. However, observationally constraining the BH spin is challenging and often subject to tension, as different measurement methods yield inconsistent spin distributions. Reflection methods in XRBs and AGN consistently measure moderate to high BH spins, $a \geq 0.5$ (Reynolds 2021; Draghis et al. 2024). In contrast, gravitational wave observatories such as LIGO-Virgo-KAGRA (LVK) consistently derive small spins, $a \leq 0.4$, from waveform data (Abbott et al. 2019; Wysocki et al. 2019; LIGO Scientific Collaboration et al. 2023; Edelman et al. 2023). Constraining and understanding spin evolution is crucial for revealing the formation pathways of LVK sources and advancing our knowledge of

binary evolution, because as much as $\sim 50\%$ of LVK sources can come from stellar binary systems. (Edelman et al. 2023).

Due to the no-hair theorem, BHs cannot hold onto the magnetic flux by themselves. Matter in the form of an accretion disk needs to force the magnetic flux into the BH and keep it there. Accretion flows can directly affect the BH spin: the accreted material adds angular momentum to the BH and leads to its spin-up. Indeed, in the Novikov-Thorne (NT) accretion disk model (Novikov & Thorne 1973), which does not include large-scale magnetic fields, the BH spins up due to accreting (Keplerian) disk’s angular momentum (Bardeen 1970; Moderski & Sikora 1996).

In jetted accretion systems, where a large scale vertical magnetic field is present, spin evolution will depend on the interplay of accretion and ejection processes near the BH event horizon. Tchekhovskoy et al. (2010) found that the jet shape determines the jet angular momentum and power fluxes and thus the spin evolution of the BH (see also Blandford & Znajek (1977)). Since the disk dimensionless thickness, h/r , or the ratio of disk height to radius, is connected to the jet opening angle, the diet of the BH affects spin evolution. Thus, the BH spin extraction can depend on the disk geometric properties, which are determined by the disk cooling regime.

The accretion rate, \dot{m} , and how close it is to Eddington value, \dot{m}_{Edd} , at which the radiation becomes as important as gravity, roughly sets the disk cooling regime (e.g., Yuan & Narayan 2014). In the highly super-Eddington regime ($\dot{m} \gg \dot{m}_{\text{Edd}}$), the disk is radiatively-inefficient and photons are trapped in the flow and advected in with the accretion flow or out with the outflow (Popham et al. 1999; Wyithe & Loeb 2012; Sądowski & Narayan 2015a; Inayoshi et al. 2016). This results in a hot accretion flow, which takes the form of a geometrically-thick accretion disk. In numerical simulations, such disks typically have a thermal scale height of $h/r \simeq 0.3 - 0.5$. The extremely sub-Eddington regime, $\dot{m} \ll 0.01\dot{m}_{\text{Edd}}$, also creates a thick radiatively-inefficient accretion flow (RIAF), which takes the form of a thick disk (Narayan & Yi 1994, 1995a,b). In the middle, $0.01\dot{m}_{\text{Edd}} \lesssim \dot{m} \lesssim \dot{m}_{\text{Edd}}$, lies the moderately sub-Eddington regime with an accretion disk that radiates efficiently and cools to thinner scale height values, which can become very small, $h/r \ll 1$.

Observations have suggested that the Eddington ratio of the BH correlates with the XRB spectral state (Esin et al. 1997, 1998; Qiao & Liu 2013; Gilfanov 2010). The so-called soft state is believed to indicate a razor-thin disk, where the inner edge of the disk is expected to approximately be at the innermost stable circular orbit (ISCO, Pringle & Rees 1972; Shakura & Sunyaev 1973a; Mitsuda et al. 1984; Marcel et al. 2019). The so-called low/hard state is linked to a thicker disk in the extremely sub-Eddington regime, with electrons

that are much cooler than the ions (Marcel et al. 2018, 2019; Liska et al. 2022).

AGN are also observed over a wide range of Eddington ratios. Generally, we expect the luminous disks to be thinner than the radiatively-inefficient disks, although the iron opacity bump and magnetic support may complicate the picture (e.g., Jiang & Blaes 2020; Jiang & Dai 2024; Hopkins et al. 2024; Squire et al. 2024; Kaaz et al. 2024). About 10% of luminous quasars are radio-loud, which seems to be related to the strength of jets (Kellermann et al. 1989; Ivezić et al. 2002; Kellermann et al. 2016). Like XRBs, the measured AGN BH spins are often large. Black hole spin estimates from standard AGN SED continuum fitting methods assume a standard accretion disk and are sensitive to inclination angle (Hagen & Done 2023; see, e.g., Davis & Tchekhovskoy 2020, for limitations of the standard disk model in the context of AGN).

More extreme accretion systems, such as collapsing massive stars producing BHs (collapsars) and binary compact object mergers, can achieve highly super-Eddington accretion rates and have thinner disks due to the effects of neutrino cooling. When neutrino luminosities are high, the disks can cool down to an aspect ratio of $h/r \sim 0.2$ (Chen & Beloborodov 2007).

For most astrophysical disks sources, accretion can occur over a wide range of Eddington ratios, resulting in a variety of disk thermal thicknesses for the same type of astrophysical source, even varying throughout the evolution of the source in some cases. This variety of disk thickness values across different types of astrophysical sources motivates a systematic exploration of the effects that disk thickness has on BH spin evolution.

For this, it is essential to capture the accretion and ejection physics, including the effects of strong magnetic fields, radiation, and curved spacetimes. This ambitious goal can be achieved with general relativistic (radiation) magnetohydrodynamic (GR(R)MHD) simulations. In this work, we focus on magnetically arrested disks (MADs, Igumenshchev et al. 2003; Tchekhovskoy et al. 2011), which are the natural end state of a disk with a sufficiently large vertical magnetic flux reservoir (Tchekhovskoy et al. 2011; Tchekhovskoy & Giannios 2015; Jacquemin-Ide et al. 2021). Such highly magnetized disk states have also been found to emerge naturally due to dynamo action within the accretion disk (Liska et al. 2020; Jacquemin-Ide et al. 2024b).

BH equilibrium spin is defined as the BH spin for which angular momentum lost through the jet balances the angular momentum and mass supplied by the disk. For thick MADs, GRMHD simulations revealed that the equilibrium spin is small, $a_{\text{eq}} \simeq 0.035 - 0.07$ (Tchekhovskoy et al. 2012; Tchekhovskoy 2015; Narayan et al. 2022; Lowell et al. 2024). Lowell et al. (2024) found that the BH only needs

to accrete 20% of its initial mass to spin down from $a = 1$ to $a = 0.2$. They also found that the BH loses most of its spin energy to the jets and that the positive angular momentum contribution from the accretion flow is suppressed by the large-scale Maxwell torques in the accretion disk (see also [Manikantan et al. 2024](#)). They then used this insight to derive a semi-analytic model for spin evolution in the thick nonradiative MAD regime. Using this model, they predicted that luminous, thin MADs would have low equilibrium spin values, $a_{\text{eq}} \sim 0.3-0.5$. This is much lower than $a_{\text{eq}} \sim 0.8$ obtained by [Ricarte et al. \(2023\)](#) based on their GRMHD simulations. Which is close to what is expected in NT disk ($a_{\text{eq}} \sim 1$ and measured in weakly magnetized standard and normal evolution (SANE) accretion disk ($a_{\text{eq}} \sim 0.9$) ([Gammie et al. 2004](#); [Chatterjee & Narayan 2022](#)).

In this work we perform high-resolution 3D GRMHD simulations of cooled BH accretion disks in the MAD state to study BH spin evolution for thin accretion disks. This allows us to extend the work of [Lowell et al. \(2024\)](#) from the radiatively-inefficient thick to luminous MADs of varying disk scale height to physically interpret our simulation results.

Section 2.1 presents the BH spin evolution equations. Section 2.3 describes our numerical setup and simulations. Section 2.4 explains how we calculate the torques on the BH. Section 3 presents our results, and, finally, Section 4 discusses the results and concludes. Throughout, we use units such that $G = c = 1$. We adopt Lorentz-Heaviside units for the magnetic field, so that the magnetic pressure is given by $p_{\text{mag}} = b^2/2$.

2. METHODS AND EQUATIONS

2.1. Spin evolution equations

Dimensionless BH spin is defined as

$$a = \frac{J}{M^2}, \quad (1)$$

where J is the angular momentum and M is the mass of the BH. The dimensionless spin spans $-1 \leq a \leq 1$. The spin evolution of the BH can be computed via a set of ODEs for the specific energy and angular momentum of the BH ([Moderski & Sikora 1996](#); [Lowell et al. 2024](#)),

$$dM = e_{\text{in}} dm \quad (2)$$

and

$$dJ = l_{\text{in}} dm, \quad (3)$$

where l_{in} and e_{in} are the specific angular momentum and energy fluxes, respectively, on the BH horizon, $r_{\text{h}} = r_{\text{g}}(1 + \sqrt{1 - a^2})$, and dm is the amount of accreted mass. Here, $r_{\text{g}} = GM/c^2$ is BH gravitational radius. Combining Equations (2) and (3) gives the ODE for the change in BH spin

with BH mass,

$$\frac{da}{d \log M} = \frac{l_{\text{in}}}{e_{\text{in}}} - 2a = \frac{s}{e_{\text{in}}}, \quad (4)$$

where \log is the natural logarithm, and we have defined the dimensionless spin-up parameter,

$$s \equiv \frac{da}{dm} M = l_{\text{in}} - 2ae_{\text{in}}. \quad (5)$$

Computing the BH spin evolution is a question of determining, as a function of BH spin, the specific fluxes, l_{in} and e_{in} , both of which depend on the (to be determined) accretion flow and jet structures.

2.2. Novikov-Thorne disk model

The NT disk model by [Novikov & Thorne \(1973\)](#) is an analytic model for a razor-thin accretion disk where the orbits are Keplerian, and the accretion mechanism is a viscosity of turbulent origin. From [Bardeen \(1970\)](#) and [Moderski & Sikora \(1996\)](#), the specific energy and angular momentum fluxes on the BH are,

$$e_{\text{in}} = \left(1 - \frac{2r_{\text{g}}}{3R_{\text{ms}}}\right)^{1/2} \quad (6)$$

and

$$l_{\text{in}} = \frac{2M}{3^{3/2}} \left(1 + 2(3R_{\text{ms}}/r_{\text{g}} - 2)^{1/2}\right), \quad (7)$$

where R_{ms} is the radius of the marginally-stable orbit, also known as the innermost stable circular orbit (ISCO). This radius is given by ([Shapiro & Teukolsky 1983](#)),

$$R_{\text{ms}}/r_{\text{g}} = 3 + Z_2 - [(3 - Z_1)(3 + Z_1 + 2Z_2)]^{1/2}, \quad (8)$$

where

$$Z_1 = 1 + (1 - a^2)^{1/3} \left[(1 + a)^{1/3} + (1 - a)^{1/3} \right], \quad (9)$$

$$Z_2 = (3a^2 + Z_1^2)^{1/2}. \quad (10)$$

2.3. Suite of MAD simulations

We carry out simulations of MADs to compute the energy and angular momentum fluxes unto the BH. For this, we use H-AMR ([Liska et al. 2022](#)), a 3D massively parallel graphical processing unit (GPU) accelerated GRRMHD code, which is based on 3D HAMRPI ([Tchekhovskoy 2019](#)) and 2D HARM2D ([Gammie et al. 2003](#); [Noble et al. 2006](#)) codes. We initialize the simulations with a torus in hydrostatic equilibrium ([Fishbone & Moncrief 1976](#)) about a BH, in a Kerr-Schild metric (see Sec. 2.3.1–2.3.3). We adopt spherical polar coordinates, r , θ , φ , and use a uniform grid in $\log r$, θ , and φ . The radial grid extends from just inside the event horizon, $R_{\text{in}} = 0.8r_{\text{h}}$, to $R_{\text{out}} = 10^5 r_{\text{g}}$ (or $R_{\text{out}} = 10^4 r_{\text{g}}$). All our simulations have at least 5 radial cells inside of the

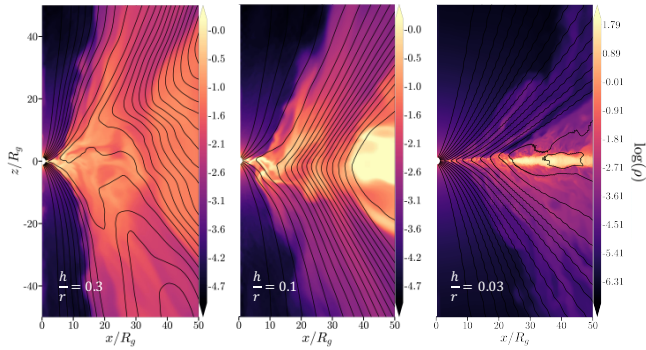


Figure 1. Smaller h/r disks (shown in yellow) are thinner and result in wider, less collimated polar jets (dark purple), as seen in the vertical slices through density for simulations with different disk scale heights, $h/r = 0.3$ (model H3a0.94hr), 0.1 (model H1a0.94), and 0.03 (model Ra0.94). Black lines, which show axisymmetric poloidal magnetic flux contours, demonstrate that both the BH and inner disk are flooded by the vertical magnetic flux, as expected in MADs.

event horizon; this ensures that the exterior of the BH is causally disconnected from the inner radial boundary of the grid. We adopt outflow boundary conditions (BCs) at the inner and outer radial boundaries, transmissive BCs at the polar boundaries, and periodic BCs in the φ -direction (Liska et al. 2022).

We insert a large poloidal magnetic flux loop into the torus, with the covariant vector potential described below. We wait for large-scale disk magnetic flux to flood the BH and lead to the MAD state (e.g., Tchekhovskoy et al. 2011).

To compute the evolution of BH spin over cosmological timescales, which are far longer than the duration of any of our simulations, we perform a suite of GRMHD simulations spanning a wide range of BH spin values. We keep the BH spin constant throughout each of the simulations, a good approximation given the extremely short duration of our simulations in the cosmological context. However, in each of the simulations, we compute the torques acting on the BH. We then use these to model the BH spin evolution by solving a set of coupled ODEs. To understand how the disk thickness affects BH spin evolution, we have run the simulations with thermal disk scale heights ranging from thick, $h/r = 0.3$, to thinner, $h/r = 0.1$ and thinnest, $h/r = 0.03$, disks. Figure 1 shows the vertical slices through density in simulations of MADs around rapidly spinning BH, $a = 0.9375$, for these three disk thickness values. We see that smaller h/r disks are thinner and result in wider jets. Whereas most of our simulations use a radiative cooling prescription (Noble et al. 2009), some use the full radiation transport scheme with a two-moment (M1) radiative closure (Liska et al. 2022). We summarize the main simulation parameters in Table 1 and discuss the simulations below in more detail.

2.3.1. Nonradiative thick MADs

To study thick MADs we utilize the simulations of Tchekhovskoy et al. (2011, 2012); Tchekhovskoy (2015) with BH spins $-0.9, -0.5, -0.2, 0.0, 0.1, 0.2, 0.5, 0.9$, and 0.99 and a polytropic index of $\Gamma = 4/3$. These simulations are denoted as $h/r = 0.3$ in Table 1. Collectively, we refer to these simulations as $h/r = 0.3$ simulations. Compared to other simulations in this paper, the Tchekhovskoy et al. (2011) simulations are lower-resolution (at most $288 \times 128 \times 128$) and shorter-duration ($t_{\text{final}} \leq 30,500 r_g/c$). Here, we have run higher-resolution ($384 \times 300 \times 64$) and longer simulations for five spin values, $a = -0.9, -0.5, 0.2, 0.5$, and 0.9375 , with a polytropic index of $\Gamma = 13/9$. Collectively, we refer to these simulations as $h/r = 0.3HR$. We show these higher-resolution thick disk MAD simulations in Table 1. Because our thick nonradiative MADs reach a thermal scale height of $h/r \approx 0.3$, we use this fiducial value to designate these simulations.

2.3.2. Cooled MADs

For two sets of models, with $h/r = 0.1$ and $h/r = 0.05$, we cool the disk to its target thickness on the Keplerian timescale using a cooling source term following Noble et al. (2009). For the initial conditions, we adopt the torus of inner radius, $r_{\text{in}} = 6.5 r_g$, and the pressure maximum radius, $r_{\text{max}} \sim 80 r_g$, where we tweak the exact value of r_{max} such that our torus extends out to an extremely large (but finite) distance, $r_{\text{out}} \sim \text{few} \times 10^4 r_g$. To quickly achieve the MAD state, we adopt the covariant vector potential, $A_\varphi = q^2$, where (EHT Code Comparison Paper, in preparation)

$$q = \frac{\rho}{\max \rho} \left(\frac{r}{r_{\text{in}}} \right)^3 \sin^3 \theta \exp \left(-\frac{r}{400 r_g} \right) - 0.2. \quad (11)$$

We then normalize the magnetic field strength such that the minimum ratio of gas to magnetic pressure is $\min \beta = 100$.

We have carried out both low- and high-resolution simulations for $h/r = 0.1$ and $h/r = 0.05$. The low-resolution runs use a base grid of $384 \times 300 \times 64$ with no grid refinement, while the high-resolution runs use a base grid of $512 \times 288 \times 256$ with one level of static mesh refinement (SMR) applied for $|\theta - \pi/2| \leq 0.315$ and $4 r_g \leq r \leq 500 r_g$, resulting in an effective resolution of $1024 \times 576 \times 512$ in the disk proper. A resolution convergence study (see Appendix A) confirms that both resolutions are adequate for $h/r = 0.1$ simulations. However, thinner disks ($h/r = 0.05$) are only resolved at the high resolution, so only the high-resolution $h/r = 0.05$ simulations are used in our analysis.

Additionally, we include a very high-resolution $h/r = 0.03$ simulation with Noble et al. (2009) cooling, previously presented in Liska et al. (2022). We refer to this simulation as model H03a0.94 and also label it as $h/r = 0.03$ 1T. Its resolution matches that of the radiative (GRRMHD) simulations (models RaX) described in Section 2.3.3. Its initial conditions are described in Liska et al. (2022).

Table 1. Simulation details. Column 1: models. Column 2: BH spin. Column 3: thermal disk scale height. Column 4: polytropic index. Column 5: total spin-up parameter. Column 6: azimuthal wedge. Column 7: base grid resolution. Column 8: effective resolution within the disk. Column 9: simulation duration. Column 10: time-averaging window. Note "*" indicates measurements on unresolved simulations performed for the resolution study described in Appendix A.

	a	h/r	Γ	s	$\Delta\varphi$	$(N_r \times N_\theta \times N_\varphi)_{\text{base}}$	$(N_r \times N_\theta \times N_\varphi)_{\text{eff}}$	$t_{\text{run}} [r_g/c]$	$t_{\text{avg}} [r_g/c]$
$h/r = 0.3$									
H3a-0.9	-0.9	0.3	4/3	5.98	2π	$288 \times 128 \times 64$	$288 \times 128 \times 64$	(0;20100)	(10000;20100)
H3a-0.5	-0.5	0.3	4/3	5.33	π	$288 \times 128 \times 32$	$288 \times 128 \times 32$	(0;16350)	(10000;16350)
H3a-0.2	-0.2	0.3	4/3	3.61	π	$288 \times 128 \times 32$	$288 \times 128 \times 32$	(0;15200)	(10000;15200)
H3a0.0	0.0	0.3	4/3	1.03	π	$288 \times 128 \times 32$	$288 \times 128 \times 32$	(0;18550)	(10000;18550)
H3a0.1	0.1	0.3	4/3	-0.5	π	$288 \times 128 \times 32$	$288 \times 128 \times 32$	(0;18725)	(10000;18725)
H3a0.2	0.2	0.3	4/3	-1.56	π	$288 \times 128 \times 32$	$288 \times 128 \times 32$	(0;13400)	(10000;13400)
H3a0.5	0.5	0.3	4/3	-4.62	π	$288 \times 128 \times 32$	$288 \times 128 \times 32$	(0;13050)	(10000;13050)
H3a0.9	0.9	0.3	4/3	-7.47	2π	$288 \times 128 \times 64$	$288 \times 128 \times 64$	(0;19900)	(10000;19900)
H3a0.99	0.99	0.3	4/3	-7.39	2π	$288 \times 128 \times 64$	$288 \times 128 \times 64$	(0;14650)	(10000;14650)
$h/r = 0.3 \text{ HR}$									
H3a-0.9hr	-0.9	0.3	13/9	6.05	2π	$384 \times 300 \times 64$	$384 \times 300 \times 64$	(0;20225)	(10000;20000)
H3a-0.5hr	-0.5	0.3	13/9	4.52	2π	$384 \times 300 \times 64$	$384 \times 300 \times 64$	(0;23250)	(10000;23250)
H3a0.2hr	0.2	0.3	13/9	-2.40	2π	$384 \times 300 \times 64$	$384 \times 300 \times 64$	(0;14800)	(10000;14750)
H3a0.5hr	0.5	0.3	13/9	-5.31	2π	$384 \times 300 \times 64$	$384 \times 300 \times 64$	(0;57825)	(52800;57800)
H3a0.94hr	0.9375	0.3	13/9	-8.67	2π	$384 \times 300 \times 64$	$384 \times 300 \times 64$	(0;68105)	(63000;68000)
$h/r = 0.1$									
H1a-0.9	-0.9	0.1	13/9	4.53	2π	$384 \times 300 \times 64$	$384 \times 300 \times 64$	(0;65055)	(60000;65000)
H1a-0.5	-0.5	0.1	13/9	3.17	2π	$384 \times 300 \times 64$	$384 \times 300 \times 64$	(0;60064)	(55000;60000)
H1a-0.2	-0.2	0.1	13/9	2.31	2π	$384 \times 300 \times 64$	$384 \times 300 \times 64$	(0;61065)	(56600;61600)
H1a0.0	0.0	0.1	13/9	1.46	2π	$384 \times 300 \times 64$	$384 \times 300 \times 64$	(0;60220)	(55200;60200)
H1a0.2	0.2	0.1	13/9	0.57	2π	$384 \times 300 \times 64$	$384 \times 300 \times 64$	(0;62400)	(57400;62400)
H1a0.3	0.3	0.1	13/9	-0.09	2π	$384 \times 300 \times 64$	$384 \times 300 \times 64$	(0;58800)	(53800;58800)
H1a0.5	0.5	0.1	13/9	-1.36	2π	$384 \times 300 \times 64$	$384 \times 300 \times 64$	(0;65600)	(60600;65600)
H1a0.94	0.9375	0.1	13/9	-3.02	2π	$384 \times 300 \times 64$	$384 \times 300 \times 64$	(0;56300)	(51300;66300)
$h/r = 0.1 \text{ HR}$									
H1a0.3hr	0.3	0.1	13/9	-0.17	2π	$512 \times 288 \times 256$	$1024 \times 576 \times 512$	(0;59400)	(45000;59400)
$h/r = 0.05 \text{ LR (warning: unresolved)}$									
H05a0.1	0.1	0.05	13/9	1.51*	2π	$384 \times 300 \times 64$	$384 \times 300 \times 64$	(0;66700)	(61700;66700)
H05a0.3	0.3	0.05	13/9	0.36*	2π	$384 \times 300 \times 64$	$384 \times 300 \times 64$	(0;55800)	(50800;55800)
H05a0.4	0.4	0.05	13/9	-0.02*	2π	$384 \times 300 \times 64$	$384 \times 300 \times 64$	(0;59380)	(54400;59380)
$h/r = 0.05 \text{ HR}$									
H05a0.4hr	0.4	0.05	13/9	-0.636	2π	$512 \times 288 \times 256$	$1024 \times 576 \times 512$	(0;45000)	(41000;45000)
$h/r = 0.03 \text{ 2T}$									
Ra0.3	0.3	0.03	5/3	0.04	2π	$1020 \times 432 \times 288$	$4080 \times 1728 \times 1152$	(188839;193162)	(188929;193162)
Ra0.4	0.4	0.03	5/3	-0.39	2π	$1020 \times 432 \times 288$	$4080 \times 1728 \times 1152$	(188839;190869)	(188889;190869)
Ra0.94	0.9375	0.03	5/3	-3.18	2π	$1020 \times 432 \times 288$	$4080 \times 1728 \times 1152$	(188839;192879)	(188889;192879)
$h/r = 0.03 \text{ 1T}$									
H03a0.94	0.9375	0.03	5/3	-2.854	2π	$1020 \times 432 \times 288$	$4080 \times 1728 \times 1152$	(188839;203339)	(188839;203339)

2.3.3. Thin radiative MADs

For even thinner MADs, we use a two-temperature (2T) radiation transport (GRRMHD) simulation of [Liska et al. \(2022\)](#) that results in a disk with a thermal scale height of $h/r \approx 0.03$. This simulation uses the M1 radiation scheme implemented in H-AMR, including Compton cooling ([Liska et al. 2022](#)). To capture the inner regions close to the BH and resolve the thin disk structure, the simulation uses adaptive mesh refinement (AMR) on a base grid of $1020 \times 432 \times 288$ cells. This resolution is then quadrupled at $5r_g \leq r \leq 120r_g$ and $|\theta - \pi/2| \leq 0.13$ to achieve an effective resolution of $4080 \times 1728 \times 1152$ cells in the disk proper. The BH spin is $a = 0.9375$. We refer to this simulation as model Ra0.94. To improve our BH spin sampling, we restart this model, Ra0.94, at $t = 188839r_g/c$ for two different spin values, $a = 0.3$ (Ra0.3) and $a = 0.4$ (Ra0.4). This is the same as the start time of our analysis of Ra0.94 (see Table 1). We refer to these simulations collectively as $h/r = 0.03$ 2T. Table 1 summarizes the resolutions and scale heights.

2.4. Calculating fluxes

We calculate the angular momentum and energy fluxes by evaluating the components of the stress-energy tensor,

$$T^{\mu\nu} = T_{\text{HD}}^{\mu\nu} + T_{\text{EM}}^{\mu\nu}, \quad (12)$$

where the hydrodynamic part is given by

$$T_{\text{HD}}^{\mu\nu} = (\rho + u_g + p_g)u^\mu u^\nu + pg^{\mu\nu}, \quad (13)$$

where ρ is the gas density, u is the internal energy, p is the pressure, all measured in the fluid frame, u^μ is the contravariant 4-velocity, and $g^{\mu\nu}$ is the contravariant metric. The electromagnetic part of the stress-energy tensor is given by

$$T_{\text{EM}}^{\mu\nu} = b^2 u^\mu u^\nu + \frac{1}{2} b^2 g^{\mu\nu} - b^\mu b^\nu, \quad (14)$$

where b^μ is the magnetic field 4-vector.

We compute the mass accretion rate,

$$\dot{m}(r) = - \int \rho u^r dA_{\theta\varphi}, \quad (15)$$

and the specific energy and angular momentum fluxes,

$$e(r) = \frac{\dot{E}(r)}{\dot{m}(r)} = \frac{1}{\dot{m}(r)} \int T_t^r dA_{\theta\varphi}, \quad (16)$$

$$l(r) = - \frac{1}{M} \frac{\dot{L}(r)}{\dot{m}(r)} = - \frac{1}{M} \frac{1}{\dot{m}(r)} \int T_\varphi^r dA_{\theta\varphi}, \quad (17)$$

where $dA_{\theta\varphi} = \sqrt{-g} d\theta d\varphi$ is the surface element, and the integrals are over a sphere of radius r . When computed at the BH event horizon, these fluxes give the prefactors in Equations (2) and (3), $l_{\text{in}} \equiv l(r = r_{\text{H}})$ and $e_{\text{in}} \equiv e(r = r_{\text{H}})$.

We also calculate the direct effect of radiation on the BH using the radiation stress-energy tensor,

$$R^{\mu\nu} = \frac{4}{3} E_{\text{rad}} u_{\text{rad}}^\mu u_{\text{rad}}^\nu + \frac{1}{3} E_{\text{rad}} g^{\mu\nu}, \quad (18)$$

where E_{rad} is the radiation energy density in the comoving frame and u_{rad}^μ is the radiation 4-velocity. We compute the radiation specific energy and angular momentum fluxes, $e_{\text{rad}}(r)$ and $l_{\text{rad}}(r)$, in the same way as in Equations (16) and (17), respectively, but where we replace T_ν^μ with R_ν^μ . We also define the radiation pressure $p_{\text{rad}} = \frac{1}{3} E_{\text{rad}}$.

We define the “jet” torque on the BH to be due to the electromagnetic components of the angular momentum and energy fluxes on the BH. We define the “disk” torque on the BH to be due to their hydrodynamic components. We also define the “radiation” torque on the BH due to $e_{\text{rad}}(r_{\text{H}})$ and $l_{\text{rad}}(r_{\text{H}})$.

Because numerical floors can add nonphysical mass density and internal energy near the horizon, we apply a magnetization cutoff on the disk torque, following the procedure described in Appendix B of [Lowell et al. \(2024\)](#). We limit the contribution from the disk such that $\sigma = b^2/\rho \leq 30$ for modes that use the density floor of $\sigma_{\text{max}} = 50$. For models with $\sigma_{\text{max}} = 15$, we choose the disk cutoff of $\sigma = 10$. We also apply a σ -cut to the radiation fluxes, as they are biased by density floors within the BH’s magnetosphere. Note that Ra0.3 and Ra0.94 include this cutoff, but Ra0.4 does not due to data loss.

We can write the total energy extraction efficiency in terms of specific energy flux e_{in} at the BH,

$$\eta = \frac{\dot{m} - \dot{E}}{\dot{m}} = 1 - e_{\text{in}} = 1 - e_{\text{HD}} - e_{\text{EM}} - e_{\text{rad}}. \quad (19)$$

3. RESULTS

Throughout this work, we differentiate simulation families of different disk scale heights by color. Gray points show nonradiative $h/r = 0.3$ simulations from [Tchekhovskoy et al. \(2011\)](#), previously analyzed in [Lowell et al. \(2024\)](#). Blue points show $h/r = 0.3$ HR models. Purple points show $h/r = 0.1$, and green points show $h/r = 0.05$ HR models. Either red or orange points show M1 2T-radiation simulations, $h/r = 0.03$ 2T. Finally, black points show the $h/r = 0.03$ 1T, which uses the [Noble et al. \(2009\)](#) cooling scheme.

3.1. Spin-up parameter and equilibrium spin

Figure 2 shows the dimensionless BH spin-up parameter, defined in Equation (20), as a function of BH spin for different disk scale heights. Each point represents a simulation, for which each s value (for a given value of spin) is the sum of the HD, EM, and radiation components:

$$s_{\text{MAD}} = s_{\text{HD}} + s_{\text{EM}} + s_{\text{rad}}. \quad (20)$$

Radiation torques are only present in simulations with radiation transport, shown in orange. The magnitude of s is an essential part of BH spin-down, as it controls the timescale at which the BH spins down to its equilibrium spin, as we discuss in Section 3.4.

The spin-up parameter for thick MADs is shown in gray, with the gray dashed line representing the semi-analytic model from Lowell et al. (2024) for nonradiative MAD spin-down. When $a \sim -1$, the BH rapidly spins up toward $a = 0$ due to a large spin-up parameter, s . As s decreases, spin evolution slows until the spin equilibrium is reached at $s = 0$. In Figure 2 the vertical lines indicate the equilibrium spin for each case, where the angular momentum and energy fluxes balance, halting further spin evolution. Thick MADs differ from NT disks, particularly at high spin ($a \sim 1$), where $s < 0$ indicates BH spin-down. As a decreases, s increases, eventually vanishing, and thus reaching equilibrium at $a_{\text{eq}} \approx 0.07$.

In contrast, thinner disks ($h/r = 0.1$, shown in purple) exhibit a spin-up parameter with a factor of ~ 2 lower magnitude at high spin. This reduction in s results in a higher equilibrium spin, $a_{\text{eq}} \simeq 0.29$, where $s(a_{\text{eq}}) = 0$, marked by the purple vertical line. While this is higher than the nonradiative disk value, it remains significantly lower than the NT disk prediction ($a_{\text{eq}} \simeq 1$). The purple dashed line represents our new semi-analytic model for spin-down in thin MADs (see Section 3.4).

Orange and green points in Figure 2 show that the magnitude of s remains largely unchanged for our thinner disks ($h/r = 0.05$ and $h/r = 0.03$) compared to $h/r = 0.1$. We find a slightly higher equilibrium spin for our thinnest ($h/r = 0.03$) disks, with $a_{\text{eq}} \simeq 0.31$. We do not have enough sampling of a to compute the equilibrium spin for $h/r = 0.05$, however, we can use the similar trends (i.e. the value of the slope, ds/da) found for simulations computed with $h/r = 0.03$ and $h/r = 0.1$ to extrapolate the value of equilibrium spin for $h/r = 0.05$: we find $a_{\text{eq}} \simeq 0.3$. This value appears consistent with the comparable disk scale heights, falling between the curves for the thinner ($h/r = 0.03$) and thicker ($h/r = 0.1$) disks. The values of equilibrium spin for our thinnest disks remain considerably lower than what is expected from razor thin NT disks.

In Appendix A, we present a resolution study for the thin disks ($h/r = 0.1$ and $h/r = 0.05$). For $h/r = 0.1$, we find that higher resolution does not affect the value of s , suggesting they yield the same a_{eq} . This implies that in our low resolution $h/r = 0.1$ simulations (models H1a#), the values of s are converged. However, for $h/r = 0.05$, higher resolution runs lead to significantly smaller values of s and result in smaller a_{eq} values – reduced from 0.4 to 0.3. We conclude that a vertical resolution of $\tilde{N}_\theta \lesssim 7$, where \tilde{N}_θ is the number of cells per scale height, is insufficient to accurately determine the equilibrium spin. High resolution in the disk proper (e.g.,

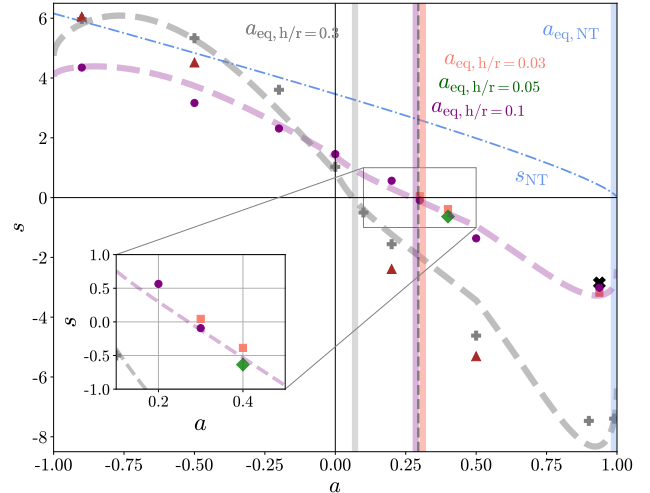


Figure 2. BH spin-down in thin MADs is less efficient than in thick MADs, resulting in a higher – but still much less than unity – equilibrium spin, a_{eq} , as revealed by the plot of spin-up parameter, s , vs. BH spin, a . The Novikov-Thorne (NT) disk spin-up curve is shown by the dash-dot blue line. The radiatively-inefficient MADs with $\Gamma = 4/3$ are shown by the gray points, their semi-analytic model from Lowell et al. (2024) is shown as the gray dashed curve. The $h/r = 0.1$ curve is shown in purple, the $h/r = 0.05$ simulation is shown in green, and the $h/r = 0.03$ curve is shown in orange for 2T and black for 1T. We also plot higher-resolution radiatively-inefficient MADs with $\Gamma = 13/9$ with brown triangles. Equilibrium spins, where each spin-up curve vanishes, are shown with vertical bars of the same color. The values of a_{eq} for all thin disks, $h/r \lesssim 0.1$, all cluster at $a_{\text{eq}}^{\text{thin}} \sim 0.3$, which is much smaller than $a_{\text{eq}}^{\text{NT}} \approx 1$ and much larger than $a_{\text{eq}}^{\text{thick}} \approx 0.07$.

via SMR) is essential for accurately determining the equilibrium spin for thin MADs. By comparing the torques between low- (under-resolved) and high-resolution (resolved) $h/r = 0.05$ simulations, we find that the main differences are in the HD components of both e_{in} and l_{in} .

Figure 3 plots the values of equilibrium spin, a_{eq} , vs. disk thermal scale height, h/r . Each point corresponds to the equilibrium spin obtained for the family of simulations for that h/r : namely, we find the $a_{\text{eq}}(h/r)$ dependence as the root of $s(a) = 0$ for that value of h/r . We find that when h/r decreases from 0.3 to 0.1, the equilibrium spin significantly increases from $a_{\text{eq}} = 0.07$ to $a_{\text{eq}} = 0.3$. Surprisingly, however, as the thermal scale height decreases further, down to $h/r = 0.05$ and 0.03, the rise in a_{eq} slows down and appears to saturate just above $a = 0.3$. To understand this puzzling feature of MAD spin-down, below we investigate: (1) why the equilibrium spin is higher in luminous MADs compared to radiatively-inefficient MADs, and (2) why the equilibrium spin converges as the disk thermal thickness decreases.

3.2. Torques on the BH

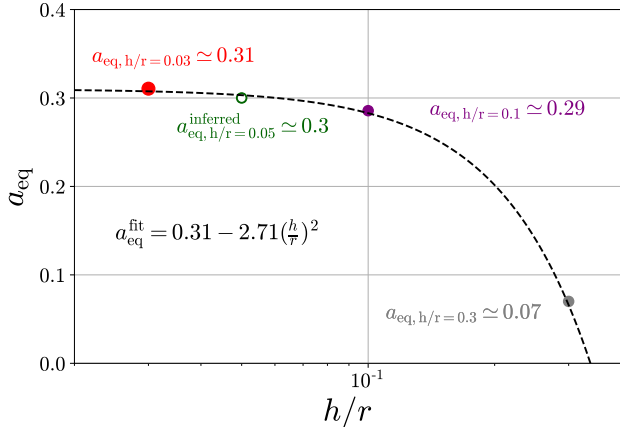


Figure 3. Equilibrium BH spin a_{eq} vs. disk scale height h/r for the four values of scale height studied in this work: 0.03, 0.05, 0.1, and 0.3. Data point colors correspondingly match those in Figure 2. As the disk cools from $h/r = 0.3$ to $h/r = 0.1$, the equilibrium spin increases. However, cooling the disk even further from $h/r = 0.1$ to $h/r = 0.05$ or 0.03 does not change the equilibrium spin significantly. The equilibrium spin appears to converge at quadratically low disk thickness. With the black dashed line we plot our fit, $a_{\text{eq}}^{\text{fit}} = 0.31 - 2.71(h/r)^2$.

Here we unravel how the different BH torque components in our MAD simulations depend on h/r . We decompose the total torques into the hydrodynamic and electromagnetic components, and subsequently into the specific fluxes that make up the spin-up parameter.

Figure 4 shows the specific angular momentum flux at the BH horizon vs. BH spin for a range of h/r . We show the NT specific angular momentum by the blue dash-dotted line. The gray dashed curves show the specific angular momentum for the thick nonradiative disks of Lowell et al. (2024). We show the angular momentum flux curves for thinner disks, with $h/r = 0.03, 0.05$, and 0.1 , in red, green, and purple, respectively.

We find that the HD angular momentum flux for thin disks is still considerably lower (by a factor ~ 2) than the angular momentum flux of an NT disk. This is consistent with our previous findings that Maxwell torques within the accretion disk lead to smaller than expected HD angular momentum fluxes unto the BH (Lowell et al. 2024). Even if the magnitude is different, the similarity in the spin dependence of l_{HD} to l_{NT} allows us to construct a simple model for this quantity. We show it as the purple dotted dashed line and describe it in Section 3.4. The HD angular momentum in thin disks is slightly larger than in thick disks: l_{HD} can be up to a factor of ~ 1.4 times larger in thin disks for negative spins.

Although our thinnest, 1T and 2T $h/r = 0.03$ MADs, (black and red open squares, respectively) lie slightly closer to the NT curve—especially when including the angular momentum from radiation in the HD torque (red filled squares)—the

difference remains small, reaching at most 25% and averaging below 10%.

Contrary to l_{HD} , the electromagnetic angular momentum flux, l_{EM} , shows a starker difference between thin and thick disks, with at most a factor of ~ 3 difference for high BH spin. Even if the magnitudes are remarkably different, the electromagnetic angular momentum flux in thin disks follows a similar trend with a as the thick disk.

For all disk thicknesses, the jets are the main component of angular momentum transport, so understanding l_{EM} is crucial to understanding BH spin-down. Furthermore, as shown above, the hydrodynamic angular momentum flux does not change enough with disk thickness to explain the difference in s for MADs of different thicknesses, as seen in Fig. 2.

Figure 5 shows both components of the specific energy flux on the BH horizon, e_{EM} and e_{HD} . The color convention for different thermal scale heights is the same as previous Figures. The top panel shows the HD component of energy. The NT disk is shown by the blue dashed line, where it drops as spin increases.

The hydrodynamic energy is lower for thin disks when compared to e_{NT} or e_{HD} for thick MADs. However, as with l_{HD} the difference between thin and thick disks for e_{HD} are at most 50% and are on average closer to 20% for most spins. The 50% difference is due to the fact that, at high spin, unlike the thick MAD which stays roughly constant with spin, the thinner disk follows a similar trend as the NT disk. The fact that e_{HD} for thin disks follows a similar trend to e_{NT} allow us again to model it as a fraction of the NT hydrodynamic energy flux, $e_{\text{HD}} = 0.85e_{\text{NT}}$.

The thinnest 1T and 2T $h/r = 0.03$ MADs (black and red open and filled squares) exhibit lower e_{HD} than the $h/r = 0.1$ MADs at moderate spin ($a \simeq 0.13$) but reach similar values at $a = 0.9375$. However, these differences never exceed 15%.

The EM specific energy fluxes also show strong differences between thin and thick disk MAD cases, slightly outshining the differential effect (between thin and thick) of the HD contribution. For high prograde spins, EM energy fluxes are about twice as small in thin MADs as in thick MADs. In contrast, for moderate and retrograde spins, the difference is less significant, with thick MADs showing only about 30–50% stronger fluxes.

3.3. Relationship between spin-down and thermal scale height

In Figure 3, we found that MADs with thinner disks ($h/r = 0.1$ or less) have a noticeably higher equilibrium spin ($a \simeq 0.3$) compared to thicker MADs with $h/r = 0.3$ ($a \simeq 0.07$).

Moderski & Sikora (1996) showed that torques applied to the BH can be decomposed into torques from the disk and jets. We write this in terms of the spin-up parameter, Equa-

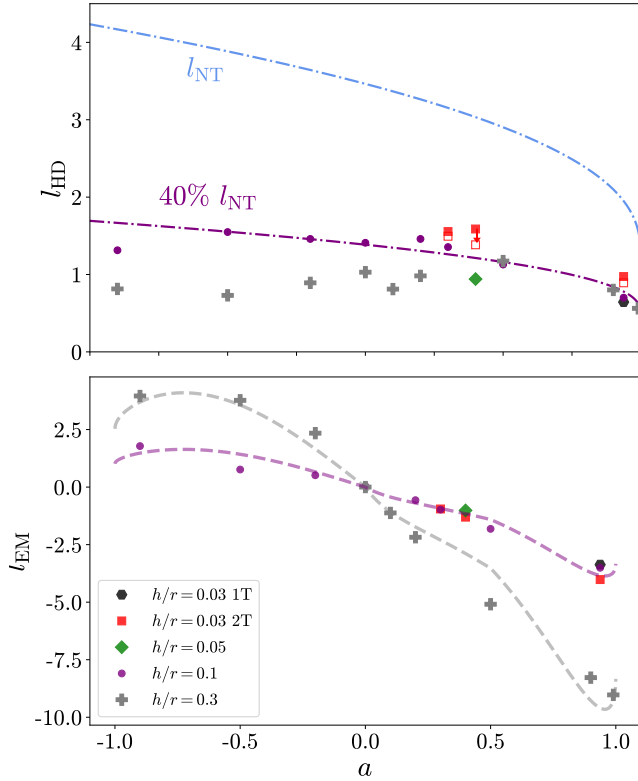


Figure 4. Our new analytic model (dashed purple lines) well describes HD and EM components of specific angular momentum supplied by thin MADs across all thicknesses, $0.03 \leq h/r \leq 0.1$. Specific angular momentum vs. spin for different disk thermal scale heights: $h/r = 0.03$ (2T red and 1T black), $h/r = 0.05$ (green), $h/r = 0.1$ (purple), and $h/r = 0.3$ (gray). [Top panel]: Hydrodynamic angular momentum flux component, l_{HD} . MADs exhibit much lower l_{HD} than the NT disk (blue dashed line). Whereas l_{HD} in thick MADs (gray) remains roughly constant, in thinner MADs l_{HD} increases with decreasing a . For $h/r = 0.1$ (purple), l_{HD} resembles the shape of l_{NT} , so we fit it with a (purple dashed) 40% l_{NT} curve, capturing the data trend well. For the thinnest disks ($h/r = 0.03$), l_{HD} values (open red squares and filled black hexagons) do not deviate significantly from the $h/r = 0.1$ results, and lie much lower than l_{NT} . Filled red squares show $l_{\text{HD}} + l_{\text{rad}}$. We note that the l_{rad} measurement for Ra0.4 does not include a σ -cutoff to account for numerical floors; σ -cutoffs for Ra0.3 and Ra0.94 indicate that l_{rad} for Ra0.4 would be lower (shown with a red downward arrow). [Bottom panel]: Electromagnetic (EM) angular momentum flux component l_{EM} . Angular momentum extraction by jets is strongest for thick MADs (gray) but weaker in cooled MADs ($h/r = 0.1$) and remains unchanged for $h/r \leq 0.1$. The semi-analytic EM models for $h/r = 0.3$ (gray) and $h/r = 0.1$ (purple dashed) are also shown.

tion (5),

$$s_{\text{MAD}} = l_{\text{HD}} - 2ae_{\text{HD}} - \eta_{\text{EM}} \left(\frac{1}{k\Omega_{\text{H}}} - 2a \right), \quad (21)$$

where we define the EM energy efficiency, $\eta_{\text{EM}} = -e_{\text{EM}}$, and the EM specific angular momentum flux on the BH, $l_{\text{EM}} =$

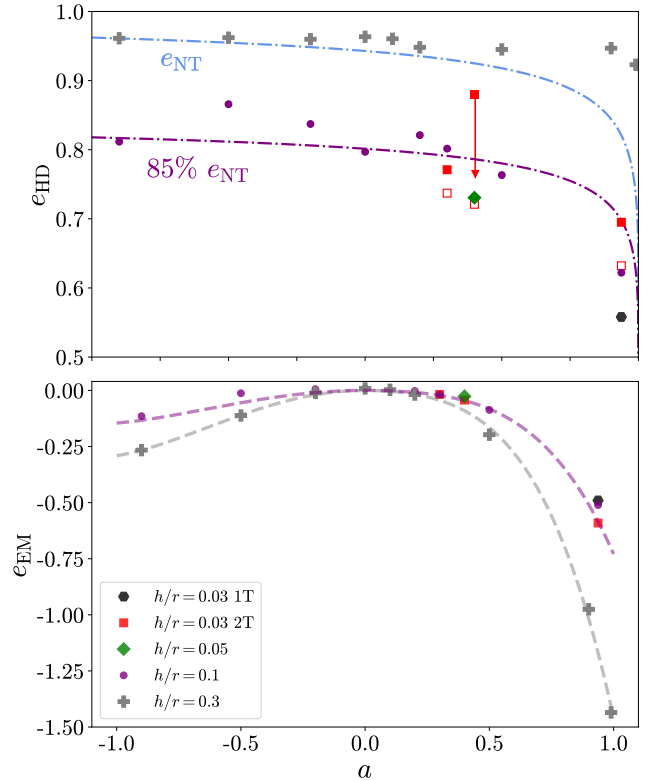


Figure 5. The analytic model (dashed purple lines) well describes HD and EM components of specific energy supplied by thin MADs across all thicknesses, $0.03 \leq h/r \leq 0.1$. Specific energy flux on the horizon vs. BH spin for varying thermal scale heights: $h/r = 0.3$ (gray), $h/r = 0.1$ (purple), $h/r = 0.05$ (green), and $h/r = 0.03$ (2T red and 1T black). [Top panel]: Hydrodynamic (HD) specific energy flux, e_{HD} . Cooled MADs with $h/r = 0.1$ contribute less HD energy to the BH. The values of e_{HD} for $h/r = 0.1$ appear to follow a similar shape vs. a as for the NT disk. We plot 85% the l_{NT} curve with the purple dashed line. The e_{HD} points for $h/r = 0.03$ (red and black) follow the same trend as e_{HD} of $h/r = 0.1$. Filled red squares show $e_{\text{HD}} + e_{\text{rad}}$. The e_{rad} measurement for Ra0.4 does not include a σ -cutoff to account for numerical floors; σ -cutoffs for Ra0.3 and Ra0.94 indicate that e_{rad} for Ra0.4 would be lower (shown with a red downward arrow). We find little difference in the e_{HD} of thin $h/r = 0.1$ and thinnest $h/r \leq 0.05$ MAD. [Bottom panel]: The purple dashed line, well-representing EM specific energy flux thin MADs is simply 1/2 the thick MAD model (gray dashed line) of Eq. of (28). MADs with spinning BHs extract energy from their BHs (when $e_{\text{EM}} < -1$). Thin MADs extract less EM energy than thick MADs. Disks with $h/r \leq 0.05$ extract similar amounts of EM energy as those with $h/r = 0.1$.

$\eta_{\text{EM}}/(k\Omega_{\text{H}})$. Here, k is the "slippage" parameter, which is the ratio of the field line angular frequency to the angular frequency of the BH horizon¹, $k = \Omega_{\text{F}}/\Omega_{\text{H}}$.

¹ We note that when $a = 0$, $\frac{1}{k\Omega_{\text{H}}}$ is undefined. However, this does not matter in practice because when $a = 0$, all EM energy and angular momentum extraction vanishes.

Because jets dominate the spin-down process and the disk influences the jet's opening angle and rotation, we explore the dynamics of jet angular momentum (k) and energy (η_{EM}), and how their interplay with the disk structure determines the equilibrium spin.

3.3.1. Weaker spin-down in thin disks

We start by comparing the jet power and efficiency for different disk thermal thicknesses. In Figure 6 we show EM efficiency η_{EM} vs. BH spin with curves for several thermal scale heights. We find that when h/r decreases from 0.3 to 0.1, the EM efficiency drops by about a factor of 2. However, when h/r decreases even further from 0.1 to 0.03, the η_{EM} decrease stalls, indicating possible convergence. Scepi et al. (2023) and Dhang et al. (2024) also found that η_{EM} drops with decreasing thermal scale height, and we find similar values of jet efficiency for $h/r = 0.1$. In contrast to Scepi et al. (2023) we find a very different jet efficiency for $h/r = 0.03$, with our jets outshining theirs by a factor of 5, although this might be due to different diagnostics for the jet efficiency.

In Figure 6 (middle panel), we show the normalized magnetic flux, $\phi_{\text{BH}} = \Phi_{\text{BH}}/\sqrt{mr_{\text{g}}c}$, where

$$\Phi_{\text{BH}} = \frac{1}{2} \int |B^r| dA_{\theta\varphi} \quad (22)$$

is the absolute BH magnetic flux, and the integral is taken over the BH event horizon. We observe that thicker disks have a larger normalized magnetic flux at the event horizon than thinner disks, consistent with previous findings (Avara et al. 2016; Scepi et al. 2023; Dhang et al. 2024). Additionally, we note that ϕ_{BH} in thin and thick disks exhibits distinct spin dependencies. Whereas thin disks show a somewhat monotonic trend with spin, thick disks display a clear maximum around $a \sim 0.3$.

We now examine whether the weaker magnetic flux in thin MADs is directly reflected in their jet power. Via the Blandford-Znajek (BZ, Blandford & Znajek 1977) mechanism, the EM jets are powered by the BH rotational energy, which leads to the following scaling for the jet power (Tchekhovskoy et al. 2010),

$$P_{\text{BZ}} = \frac{\kappa}{4\pi c} \Omega_{\text{H}}^2 \Phi_{\text{BH}}^2 f(\Omega_{\text{H}}), \quad (23)$$

where κ is a constant that depends on the magnetic field geometry, c is the speed of light, $\Omega_{\text{H}} = a/r_{\text{H}}$ is the BH rotational frequency. Here Φ_{BH} is the magnetic flux threading the BH event horizon, and $f(\Omega_{\text{H}}) = 1 + 1.38(\Omega_{\text{H}}r_{\text{g}}/c)^2 - 9.2(\Omega_{\text{H}}r_{\text{g}}/c)^4$ is a high-spin correction. Here we use the value $\kappa = 0.054$ for a jet with a split-monopole geometry.

We observe in Eq. (23) that the BZ jet power is a function of Φ_{BH}^2 , κ and a . To explain why jets are less powerful in luminous MADs than in nonradiative MADs, the bottom panel of Figure 6 shows the EM power normalized by

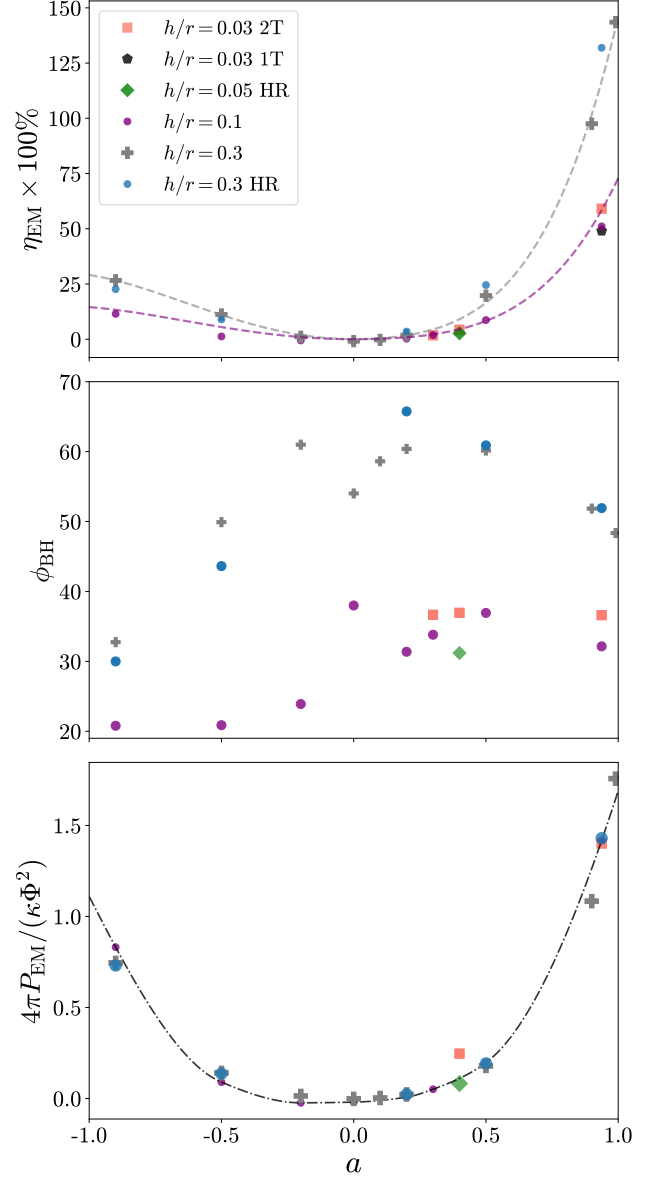


Figure 6. [Top panel]: Electromagnetic (EM) efficiency vs. BH spin for varying h/r . At high spin, the EM efficiency of radiatively-inefficient MADs is roughly twice that of the MADs cooled to a thermal scale height of $h/r = 0.1$. For the thinnest disks with $h/r = 0.03$, the EM efficiency is roughly the same as the ones with $h/r = 0.1$. [Middle panel]: Magnetic flux on the event horizon of the black hole normalized to \sqrt{m} , also called MADness parameter. We notice that thin MADs have a smaller fluxes at the event horizon. [Bottom panel]: Electromagnetic (EM) power normalized to magnetic flux on the BH horizon vs. BH spin for simulations with varying disk scale height. The gray dot-dashed line is a spline interpolation for $h/r = 0.1$ points, included solely to guide the reader's eye. Although in Figure 6, EM efficiency for $h/r = 0.1$ is about 50% that of $h/r = 0.3$, the magnetic flux-normalized jet power of all thermal scale heights (or Eddington ratios) are equivalent. Thus, the lower EM power in cooled disks is a result of lower magnetic flux on the BH.

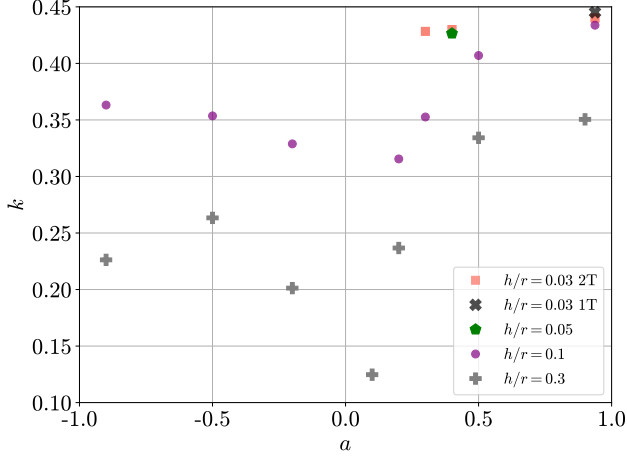


Figure 7. $k = \Omega_F/\Omega_H$ as a function of BH spin. The gray points show the values calculated in [Lowell et al. \(2024\)](#), and the colored points show cooled disks of various scale heights. For any value of spin, thick, radiatively-inefficient disks have jets with the lowest angular frequency. As the disk cools, the value of k increases. k appears to converge as the disk becomes thinner.

$\frac{1}{4\pi}\kappa\Phi_{\text{BH}}^2$, with $\kappa = 0.054$, isolating the spin dependence of the jet power. Here, we measure the EM (jet) power P_{EM} as the EM component of the total energy flux, $\dot{E}(r)$ (Eq. 16, on the BH (not normalized to the mass flux).

Surprisingly, once normalized to the magnetic flux on the BH, the EM power becomes the same for all disk thermal scale heights. Thus, it is Φ_{BH} that sets the jet power, with thinner disk having lower values of Φ_{BH} . However, what sets Φ_{BH} or ϕ_{BH} is largely unknown.

Now we look at the angular momentum extraction due to the EM jets. As we saw in Figure 4, l_{EM} has a steep dependence on the thermal scale height, changing substantially when going from $h/r = 0.3$ to $h/r = 0.1$. Following [Moderski & Sikora \(1996\)](#) and [Lowell et al. \(2024\)](#), we can describe the EM specific angular momentum flux on the BH as $l_{\text{EM}} = \eta_{\text{EM}}/(k\Omega_H)$ to better understand its behavior.

In Figure 7 we show the "slippage" parameter, k , as a function of spin for the different disk thicknesses. We see that the thinner the disk, the larger the value of k . A higher k , indicating faster rotation of field lines, results in less efficient angular momentum extraction and thus a lower l_{EM} . For a MAD of a given h/r , this leads to a higher equilibrium spin.

The rotation velocity of the magnetic field lines, k , is tied to the jet's structure, making it useful to examine the magnetic field lines connected to the BH in order to understand BH spin-down. In Figure 8 we plot the outermost magnetic field line attached to the BH averaged in time and φ . This field line represents the jet shape at the boundary where it interacts with the wind. One can approximate the flux of a collimating field line as a power-law in distance ([Tchekhovskoy et al.](#)

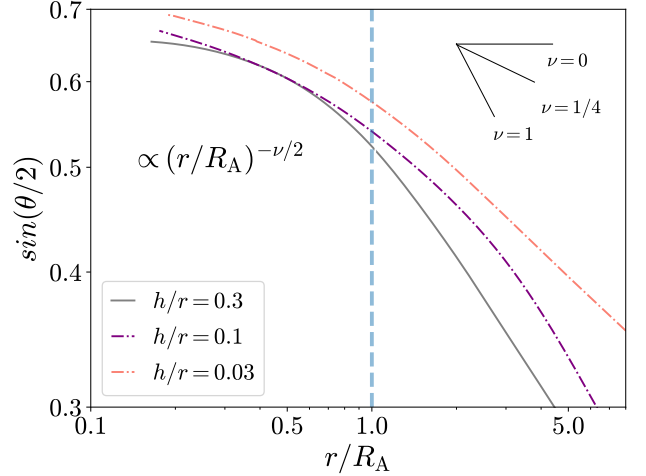


Figure 8. Last magnetic field line attached to BH with spin $a = 0.9375$ for three simulations of varying scale height. We normalize the radial coordinate to the Alfvén radius, $R_A = r_g/\Omega_F$, also shown by the vertical blue line. For a distance greater than roughly $R_A \sim 8r_g$ we find that the thinner the disk, the wider the jet opening angle. See Figure 7, where thin disks have a larger value of $k = \Omega_F/\Omega_H$, implying that jets with a wider opening angle have jets that are rotating faster than more collimated jets. We notice that both thick disks are parallel to each other and therefore have similar ν while the thick disk has a larger ν . We show the high resolution simulation for $h/r = 0.3$ (H3a0.94hr).

2010),

$$a_\varphi = r^\nu (1 - \cos \theta), \quad (24)$$

where ν sets the jet shape: $\nu = 0$ corresponds to monopolar and $\nu = 1$ to parabolic jet. In a realistic jet, the flux will not follow such a simple power-law. Nevertheless, we can use this approximation to understand the relationship between the jet shape and jet angular momentum flux. From Eq. (24), it follows that

$$\sin\left(\frac{\theta}{2}\right) = \sqrt{\frac{a_\varphi}{2}} \left(\frac{r}{R_A}\right)^{-\nu/2}, \quad (25)$$

where θ is the polar angle, a_φ is the enclosed magnetic flux, constant along the field line, r is the distance from the black hole, and ν is a parameter describing the jet shape that we generalize to depend on radius. We normalize the distance to the Alfvén radius, $R_A = 1/\Omega_F$, where the Alfvén velocity is equal to the outward velocity of the gas. At the Alfvén surface the outflowing material can no longer communicate back to the event horizon through Alfvén waves. Indeed, only the jet shape inside of the Alfvén surface can affect the jet launching and hence, the value of k . Therefore, the Alfvén surface defines a meaningful radius where we can compare the value of ν for different simulations.

We show jet shapes for models with $a = 0.9375$ of $h/r = 0.3, 0.1, 0.03$ using gray, purple, and orange curves, respec-

tively. For each model, we use the value of k (shown in Figure 7) to compute R_A .

We find that the thinner the accretion disk, the wider the jet barrel at the Alfvén radius. The value of ν at R_A for the thick disk is close to ~ 1 , whereas the value for the two thinner disks ($h/r = 0.1$ and $h/r = 0.03$) is around $\sim 1/4$. We can also see this from Figure 1: disks with smaller thermal thickness collimate jets less than thicker disks. The thinner the disk, the greater the jet opening angle, with magnetic field lines increasingly resembling a monopole geometry ($\nu = 0$) as scale height decreases. Thinner disks allow more space for jet widening, and MHD acceleration becomes most efficient with larger lever arms. As a result, field lines rotate more rapidly (with a larger Ω_F and consequently greater k , as seen in Figure 7).

This picture is consistent with the work of Tchekhovskoy et al. (2010) who studied k as a function of the index ν , and found that different jet geometries lead to different values of k . A monopole ($\nu = 0$) leads to a roughly constant $k \sim 0.5$, while a parabolic geometry ($\nu = 1$) leads to a k that decreases with angle and has an average value² of ~ 0.4 . We conclude that larger time-averaged values of k are consistent with jet shapes approaching a monopole as h/r decreases. We also stress that the change in k and jet power is the strongest between $h/r = 0.3$ and $h/r = 0.1$. The change between $h/r = 0.1$ and $h/r = 0.03$ is almost imperceptible, which is consistent with their slopes being the same at the Alfvén surface.

3.3.2. Decoupling of thermal and magnetic dynamics

As the thermal scale height decreases in Figure 3, a_{eq} appears to converge. This could imply that for even thinner disks, the equilibrium spin might continue to asymptotically approach a relatively small value of spin $a \lesssim 0.31$, much lower than the analytic value for NT razor-thin disks, $a = 0.998$. For the thermal scale height to drop from $h/r = 0.1$ to $h/r = 0.03$ and leave the spin evolution unchanged, some physical property of the disk structure needs to remain independent of the scale height at $h/r \lesssim 0.1$. As we show below, the magnetic structure and magnetic forces are roughly independent of the thermal scale height for $h/r \lesssim 0.1$.

In thin MADs, magnetic pressure—both its large-scale and turbulent components—controls the vertical equilibrium of the accretion disk, and thermal pressure becomes highly subdominant. This may explain why BH spin-down by thin MADs is unaffected by the thermal h/r value: this is because the primary torque on the BH comes from the jet’s magnetic fields, which appear to remain unchanged for $h/r \leq 0.1$.

We begin by examining the thermal and magnetic forces governing disk compression and expansion in the latitudinal (θ) direction, disregarding centrifugal force since it is

unrelated to jet formation, BH energy and angular momentum extraction, or thermal h/r . While thermal and radiation pressures act to expand the disk, magnetic pressure plays a more complex role. Turbulent and large-scale (laminar) magnetic pressures contribute differently to the disk dynamics, influencing its overall equilibrium in distinct ways. Turbulent magnetic pressure arises from disk turbulence, providing support against collapse, whereas large-scale (laminar) magnetic pressure results from fields anchored to the jet structure, compressing the disk. One can separate both terms using a Reynolds decomposition,

$$\langle \delta b^2 \rangle_{t,\varphi} = \langle b^2 \rangle_{t,\varphi} - \langle b \rangle_{t,\varphi}^2, \quad (26)$$

where brackets are averages in both time and φ , $\langle \delta b^2 \rangle_{t,\varphi}$ is the turbulent magnetic pressure, $\langle b \rangle_{t,\varphi}^2$ is the large-scale (or laminar) magnetic pressure, and $\langle b^2 \rangle_{t,\varphi}$ is the total magnetic pressure.

We show the θ -profiles of the magnetic pressures and the thermal pressure in Figure 9 for the model H1a0.94. We see that the thermal and turbulent magnetic pressures have similar vertical profiles, whereas the large-scale laminar magnetic pressure has an inverted profile. The reason for this difference is that $\langle \delta b^2 \rangle_{t,\varphi}$ and $\langle b \rangle_{t,\varphi}^2$ play different roles³: (1) the laminar magnetic pressure from the jet compresses the disk and (2) the turbulent magnetic pressure, along with the thermal pressure, resists the disk compression and maintains the magnetohydrostatic equilibrium. In radiative simulations, the radiation pressure also resists disk compression, as expected. The compressive role of $\langle b \rangle_{t,\varphi}^2$ is an established result from self-similar theory (Ferreira & Pelletier 1995), and the role of the turbulent magnetic pressure on the vertical equilibrium is consistent with previous 3D (GR)MHD simulations (Salvesen et al. 2016; Jacquemin-Ide et al. 2021; Scepi et al. 2023). Similar vertical pressure profiles are observed across all simulations at all radii, modulated by disk thickness; thicker disks exhibit broader pressure profiles. However, the relative magnitudes of the various pressures depend on disk thickness.

We now focus on how the relative magnitudes of the pressures depend on the disk thickness. In Figure 10 we plot the ratio of the turbulent magnetic pressure to the sum of the thermal and radiation pressures in the disk mid-plane for three simulations with $a = 0.9375$ and $h/r = 0.3, 0.1, \text{ and } 0.03$, shown as gray, purple, and orange lines, respectively. Since these pressures all act to expand the disk, this ratio indicates the dominant pressure support mechanism for the accretion disk. A clear dichotomy emerges between thick ($h/r = 0.3$)

² We note that, in Tchekhovskoy et al. (2010) k never dropped below 0.25.

³ Explicit compression and expansion can be understood by examining the inverse of the gradient of the various terms in Fig. 9. A positive gradient, $P(\theta_2) - P(\theta_1) > 0$ where $\theta_1 = \pi/2$ and $|\theta_2 - \pi/2| > 0$, results in compression, while a negative gradient, $P(\theta_2) - P(\theta_1) < 0$, leads to expansion.

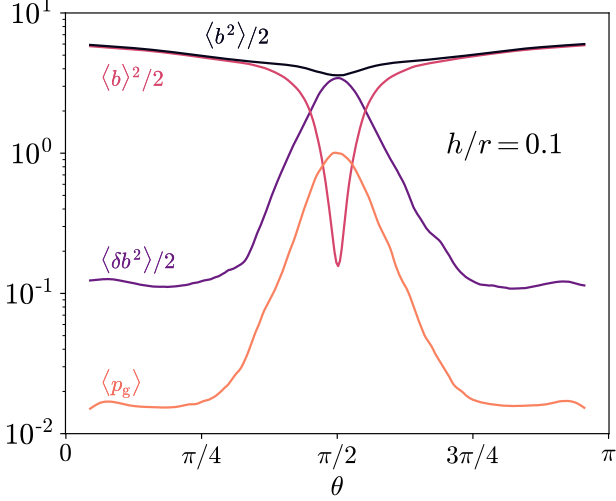


Figure 9. Vertical profiles at $r = 6r_g$ of time-averaged magnetic pressures for H1a0.94 normalized to thermal pressure in the midplane. Large-scale laminar magnetic pressure (magenta) dominates over turbulent magnetic pressure (purple) and thermal pressure (orange) above and below the disk. Turbulent magnetic pressure dominates the disk midplane.

and thin disks ($h/r = 0.1$ and $h/r = 0.03$). Thin disks are magnetically dominated at the midplane over a larger range of radii, $r \lesssim 15r_g$ compared to thick disks, which are only magnetically dominated at $r \lesssim 3r_g$. We conclude that thin disks are supported primarily by turbulent magnetic pressure, whereas thick disks are thermally supported, aligning with previous findings (Scepi et al. 2023). This shows that the disk thermal scale height is now decoupled from the disk vertical equilibrium and thus is not a relevant quantity for characterizing the system.

In Section 3.3.1, we demonstrated that jet shape (parabolic or monopolar) directly determines the k factor, playing a key role in regulating the jet angular momentum flux from the BH. We also found that simulations with $h/r = 0.1$ and $h/r = 0.03$ exhibit identical jet shape slopes, both forming monopolar-like jets, whereas thick disks produce parabolic jets. Geometric arguments suggest a connection between jet morphology and disk thermal thickness, which we propose is mediated by the compression of the disk by the large-scale magnetic field attached to the jet.

To show this, we examine the density-normalized vertical compression force exerted by the pressure of the large-scale magnetic field, $\langle b \rangle_{t,\varphi}^2$, on the accretion disk defined as,

$$F_{\text{b,jet}} = -\frac{1}{\langle \rho \rangle_{t,\varphi}} \partial_\theta (\sqrt{-g} \langle b \rangle_{t,\varphi}^2 / 2). \quad (27)$$

We divide by the local density, as magnetic acceleration and compression strength depend on density, with lower densities enabling more efficient acceleration. Curvature terms are ig-

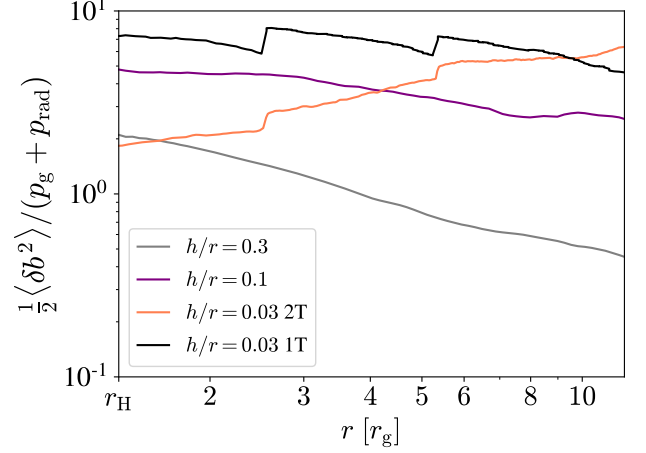


Figure 10. Ratio of turbulent magnetic pressure to thermal and radiation pressures measured in the equatorial plane for varying disk scale heights with BH spin of $a = 0.9375$. The thick MAD (gray) is dominated by magnetic pressure in the inner few radii, but thermal pressure dominates beyond $4r_g$. The cooled MAD (purple) is dominated by magnetic pressure overall. Magnetic pressure also dominates in Ra0.94, increasing with radius until $\frac{1}{2} \langle \delta b^2 \rangle / (p_g + p_{\text{rad}}) > 6$ at $10r_g$. We show the high resolution simulation for $h/r = 0.3$ (H3a0.94hr).

nored, as they are found to be negligible. We also ignore the vertical (θ) magnetic tension forces, as we also find them to be negligible (this is not the case for radial tension forces, see Chatterjee & Narayan 2022).

In Figure 11, we present $F_{\text{b,jet}}$, the density-normalized compression force measured at $r = 3r_g$, for four simulations with $a = 0.9375$: $h/r = 0.3$, $h/r = 0.1$, $h/r = 0.03 \text{ 2T}$, and $h/r = 0.03 \text{ 1T}$ shown as gray, purple, orange and black lines, respectively. Arrows indicate the force direction: a positive force pushes along θ , while a negative force pushes in the opposite direction. All simulations exhibit similar profiles, showing compression towards the disk midplane above and below it and an expansion region above and below the compression zone. We associate the expansion region with jet expansion and confinement; however, this is not our region of interest. The magnitude of disk compression reveals a dichotomy between the thin ($h/r = 0.1$ and $h/r = 0.03$) and thick ($h/r = 0.3$) disks: thicker disks display stronger compression above and below the disk midplane. Furthermore, all simulations of thin disks show roughly similar disk compression magnitudes, even though their disk thicknesses differ by a factor of 3.

We find stronger disk compression for thicker disks, because thicker disks restrict the jet expansion, resulting in a stronger backreaction against the disk. When the disk becomes sufficiently thin ($h/r \leq 0.1$), further thinning has minimal impact since the jet occupies most of the available space. The twofold increases in $F_{\text{b,jet}}$ compression for thicker vs.

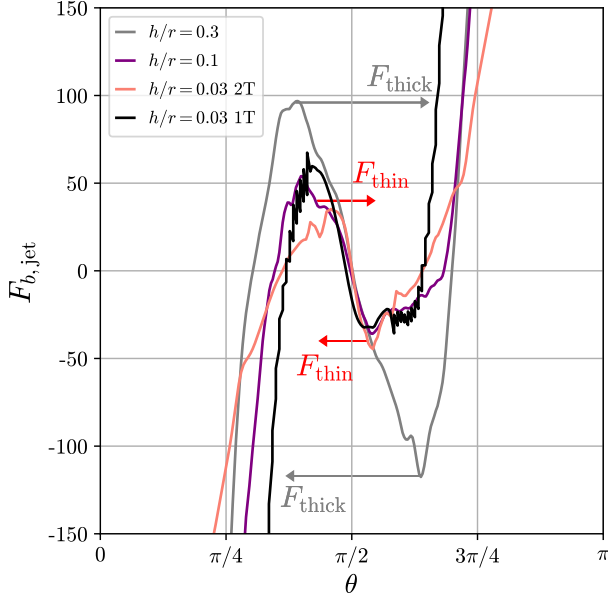


Figure 11. All thin MADs, $0.03 \leq h/r \leq 0.1$, experience comparable magnitude of magnetic compression. In contrast, for thick MADs ($h/r = 0.3$), compression is twice as strong: $F_{\text{thick}} \sim 2F_{\text{thin}}$. This is consistent with thicker disks producing more powerful jets that compress the disk more. The density-normalized compression force, $F_{b,\text{jet}}$, due to the large-scale magnetic field is shown as a function of θ , defined in Eq. (27) and measured at $r = 3 r_g$. Red arrows indicate the force direction, with positive forces pointing along θ and negative forces pointing against it. We show the high resolution simulation for $h/r = 0.3$ (H3a0.94hr).

thinner disks is consistent with the twofold increase in jet efficiency observed in Fig. 6 for thicker vs. thinner disks⁴.

We conclude that when the disk thickness falls below a certain threshold, the disk properties are determined more strongly by the disk magnetic field structure than by the disk thermodynamics. This is evidenced by the minimal differences in $F_{b,\text{jet}}$, η_{EM} , k , and $\frac{1}{2}\langle\delta b^2\rangle/(p_g + p_{\text{rad}})$ between simulations with $h/r = 0.1$ and $h/r = 0.03$. Consequently, we suggest that this is why the equilibrium spin, a_{eq} , converges as the disk thickness decreases. For disk thickness values below $h/r \sim 0.1$, jet properties become decoupled from the disk thermodynamics, because magnetic forces dominate over thermal forces.

3.4. Semi-analytic model for BH spin-down in cooled MADs

Lowell et al. (2024) developed a physically-motivated semi-analytic model that describes BH spin-down in

⁴ The fact that $F_{b,\text{jet}}$ is strongest for thick disks may seem at odds with thinner disks being more highly magnetized at the midplane (see Fig. 10). However, the ratio $\frac{1}{2}\langle\delta b^2\rangle/(p_g + p_{\text{rad}})$ can be misleading for comparing magnetic field strength across simulations, as thermal (and radiative) pressure also changes with h/r .

radiatively-inefficient MADs. Using our new suite of simulations of luminous MADs with varying h/r , we now construct a model for thinner MADs.

In panels (a) of both Figures 4 and 5, we find that e_{HD} follows a curve of $0.85e_{\text{NT}}$, and l_{HD} follows $0.4l_{\text{NT}}$. Thus, we can model the hydrodynamic disk component of cooled MADs as follows: $s_{\text{HD,cool}} = 0.4l_{\text{NT}} - 0.85e_{\text{NT}} \times 2a$.

The electromagnetic jet component also follows an interesting trend that is straightforward to model. As we showed in Section 3.3, η_{EM} for $h/r = 0.1$ follows a curve that is approximately $1/2$ of η_{EM} for thick MADs. Thus, we can use the fit from Lowell et al. (2024) and model η_{EM} for thin disk as $\eta_{\text{EM}}^{\text{thin}} = \frac{1}{2}\eta_{\text{EM}}^{\text{thick}}$, where

$$\eta_{\text{EM}}^{\text{thick}} \times 100 = \begin{cases} -19.8a^4 + 48.9a^2, & a \leq 0, \\ 106.3a^4 + 39.5a^2, & a \geq 0. \end{cases} \quad (28)$$

Figure 6 (top) shows that our model for η_{EM} above well reproduces the jet efficiency for thin disks.

We fit the spin-dependence of the k factor using the data shown in Fig. 7, with a power law⁵,

$$k_{\text{thin}} = \begin{cases} 0.16|a|^{0.15} + 0.2, & a < 0 \\ 0.24a^{0.4} + 0.2, & a > 0. \end{cases} \quad (29)$$

Figure 4, shows that our fit for $l_{\text{EM}} = \frac{1}{k_{\text{thin}}\Omega_H}\eta_{\text{EM}}^{\text{thin}}$, as a function of a , reproduces the simulation data well. By combining EM and HD components, we obtain the full semi-analytic model,

$$s_{\text{MAD,thin}} = 0.4 \times l_{\text{NT}} - 0.85 \times e_{\text{NT}} \times 2a - \frac{\eta_{\text{EM}}^{\text{thick}}}{2} \left(\frac{1}{k_{\text{thin}}\Omega_H} - 2a \right), \quad (30)$$

for BH spin-down in cool MADs. Figure 2 shows our spin evolution model (Eq. 30) with the purple dashed line, which reproduces the simulation data well. Although this model is tailored to $h/r = 0.1$, it also well reproduces the behavior of s for thinner disks, thanks to the universality of thin MAD structure (see Section 3.3).

3.5. BH spin-down timescales

Figure 12 shows BH spin evolution as a function of mass accreted onto the BH for thin MADs with $h/r = 0.1$. For this, we solve the coupled ODEs, Equations (2) and (4), and use spline interpolations for the specific energy and angular momentum fluxes at the horizon, for simulations (solid lines) with $h/r = 0.1$ (models H1a#). We show solutions for the

⁵ In this definition, we set $k(a=0) = 0.2$, though strictly speaking, $k(a=0)$ is undefined. This choice, made for the quality of the fit, does not affect our results since the angular momentum extraction term goes to zero when $a=0$, as $\eta_{\text{EM}}(a=0) = 0$.

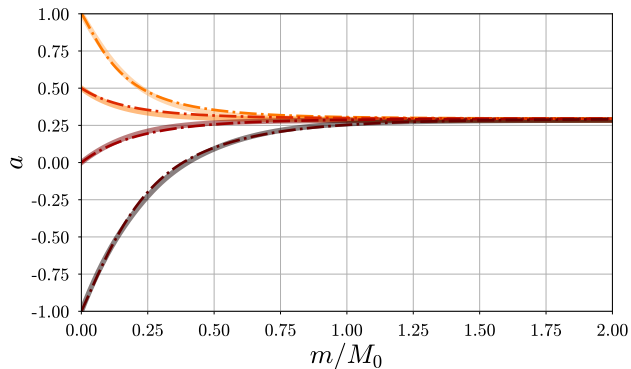


Figure 12. Our semi-analytic model (dashed lines) accurately describes BH spin evolution in thin MADs. BH spin evolution $a(m/M_0)$ for thin MADs with $h/r = 0.1$ (models H1a#). Here, m is the accreted mass and M_0 is the initial mass of the BH. When $m/M_0 = 1$, the BH has accreted its own (initial) mass. We show solutions for the initial spin values $a_0 = -1, 0, 0.5$, and 1 , for any initial spin, the BH will evolve to an equilibrium spin of $a_{\text{eq}} \approx 0.29$. For an initial spin of $a = 1$, the BH of a thin MAD will spin down to $a = 0.5$ after accreting 25% of its initial mass. For most initial spins, the BH must accrete around 85% to reach equilibrium spin. For negative initial spin, the BH must accrete more mass than the positive initial spin to reach a_{eq} , roughly 125% of M_0 . Dashed lines, which show the spin evolution using the semi-analytic model (Eq. 30), agree well with the MAD spin-down model, which uses spline fits to e_{in} and l_{in} .

initial spin values $a_0 = -1, 0, 0.5$, and 1 . We find that regardless of the initial spin, a evolves to an equilibrium value of $a_{\text{eq}} \approx 0.3$. Most initial spins equilibrate after the BH has accreted 85% of its initial mass, while $a_0 = -1$ requires 125% accretion to reach equilibrium. Thin MADs with $a = 1$ spin down to $a = 0.5$ after accreting 25% of the initial BH mass, a slower process compared to thick MADs, which only require the accretion of 10% of the BH mass for the same spin-down. We also solve the ODEs using our thin MAD model (Equation 30, dashed lines) and confirm that our model reproduces the simulation (solid lines) well. We associate the reduced BH spin-down efficiency in thin MADs with a general decrease in angular momentum and energy extraction by the jets (see Section 3.3).

4. SUMMARY AND DISCUSSION

4.1. Summary

In this study, we performed 3D GRMHD simulations of thin, luminous MADs with various disk thicknesses to investigate BH spin evolution. Previous works found that thick, nonradiative MADs result in low equilibrium spin values, $a_{\text{eq}} \approx 0.07$ for polytropic index $\Gamma = 4/3$ (Tchekhovskoy et al. 2011; Lowell et al. 2024) and $a_{\text{eq}} \approx 0.035$ for $\Gamma = 13/9$ (Narayan et al. 2022; Lowell et al. 2024). Our findings reveal, for the first time, that even in cooled MADs, the BH spin reduces down to a small equilibrium spin value of $a_{\text{eq}}^{\text{thin}} \approx 0.3$.

Interestingly, we observe that from $h/r = 0.1$ to $h/r = 0.03$, the difference in the equilibrium spin is negligible. This suggests that the equilibrium spin converges to a universal value, $a_{\text{eq}} \approx 0.3$. This is in stark contrast to the equilibrium spin of $a_{\text{eq}} \approx 1$ for the analytic NT disk. Ultimately, it is straightforward to achieve a low BH spin in a system that accretes a significant amount of mass in the MAD state, be it of the luminous or nonradiative variety. Here, we used the physical model of Lowell et al. (2024) to decompose the torques of cooled MADs and analyze their BH spin evolution. As with thick MADs, the jet electromagnetic torques remain the dominant spin-down mechanism. However, we find that the higher equilibrium spin, by a factor of four, in thin MADs ($h/r \leq 0.1$) relative to thick MADs ($h/r = 0.3$) is due to less efficient jet-driven energy and angular momentum extraction from the BH. Specifically, jets in thin MADs are half as energetically efficient as those in thick MADs. Further, thin MADs have EM angular momentum torques up to two times weaker than thick MADs, for the same jet efficiency. We attribute this reduced efficiency in jet-driven angular momentum extraction to differences in jet shape between thin and thick MADs. Whereas thick MADs produce parabolic jets, thin MADs generate monopolar jets, which are less efficient at angular momentum extraction for the same jet energy efficiency.

We present a new semi-analytic spin-down model that accurately reproduces the spin-down timescale and equilibrium spin of thin MADs with $h/r \leq 0.1$. We find that in a thin MAD, a BH with an initial spin of $a = 1$ spins down to $a = 0.5$ after accreting just 25% of its initial mass. This is a factor of 2.5 larger than for thick ($h/r = 0.3$) MADs. Most initial spins reach equilibrium after accreting 85% of the BH's initial mass, while $a = -1$ equilibrates after accreting 125%.

Our results indicate that some persistent MAD physical property ensures the universality of the equilibrium spin for thermal scale heights less than $h/r = 0.1$. We propose that the explanation lies in the balance between thermal, radiation, and magnetic (large-scale or turbulent) pressures. Whereas thick MADs are thermally-supported, thin MADs (thermal $h/r \leq 0.1$) are supported by the turbulent magnetic pressure (as also found by Scepi et al. (2023)). Furthermore, we find that in such thin MADs the vertical compression of the disk by the large-scale magnetic field pressure, associated with the jet-launching, becomes independent of the disk thermal thickness. This suggests that the overall magnetic structure, which governs most of the BH spin-down, decouples from the accretion disk thermal properties for $h/r \leq 0.1$. In such thin MADs, the decoupling of thermal and magnetic pressures (large-scale or turbulent) may explain why the equilibrium BH spin settles at a universal, low value, $a_{\text{eq}} \approx 0.3$, independent of the disk thickness.

Our resolution tests (Appendix A) show that under-resolving thin MADs with $h/r = 0.05$ leads to a significantly higher equilibrium spin. We find that a vertical resolution of $\tilde{N}_\theta \lesssim 5$, where \tilde{N}_θ is the number of cells per scale height, is insufficient to accurately determine the equilibrium spin⁶. This discrepancy arises from the artificially increased hydrodynamic energy and angular momentum fluxes in lower-resolution runs, leading to $a_{\text{eq}} \approx 0.4$ for $\tilde{N}_\theta \approx 5$ and $a_{\text{eq}} \approx 0.3$ for $\tilde{N}_\theta \approx 9$. We emphasize that high resolution is essential for accurately modeling spin evolution in thin MADs.

It is possible that for even thinner disks, perhaps an order of magnitude thinner in h/r , magnetic and thermal pressures remain permanently decoupled. Alternatively, disk dynamics may still depend on h/r , reaching a critical value where the disk can no longer retain its magnetic flux (Lubow & Spruit 1995). In that scenario, the disk would transition toward the NT state, theoretically contributing to BH spin-up. Observational evidence, such as jet quenching in the razor-thin XRB soft state, may support this idea. In contrast to thin MADs, which are dominated by super-thermal mainly turbulent magnetic fields at the midplane accretion disks dominated by super-thermal toroidal fields (which is different from MADs) appear to be influenced by their thermal thickness, even if p_g is not dynamically relevant for the disk vertical equilibrium (Squire et al. 2024).

We compute a simple fit for the dependence of a_{eq} on disk thickness, finding $a_{\text{eq}} \simeq 0.31 - 2.7(h/r)^2$. This provides a rough estimate of how a_{eq} might vary with the Eddington ratio, $\lambda_{\text{Edd}} = \dot{m}/\dot{m}_{\text{Edd}}$, and clearly shows that the equilibrium spin plateaus at $a_{\text{eq}} \lesssim 0.31$. In future work, we plan to extend this model across a broader range of Eddington ratios.

4.2. Comparison with other work

Although our work is the first to measure BH spin-down for cooled thin MADs with $h/r \leq 0.1$, previous studies have already examined jet efficiency in such disks (Avara et al. 2016; Scepi et al. 2023; Dhang et al. 2024). For $h/r = 0.1$, our results broadly agree with prior findings, showing similar jet efficiencies and magnetic fluxes at the event horizon. However, for even thinner disks ($h/r \sim 0.03$), our measured jet energy efficiencies differ significantly, with Scepi et al. (2023) reporting jet efficiencies a factor of 5 lower. This discrepancy may stem from the differences in the measurement methods, as Scepi et al. (2023) evaluates jet power at larger distances rather than the event horizon. Nonetheless, we note that our measurement of magnetic flux at the horizon, ϕ_{BH} , is consistent with Scepi et al. (2023), even for MADs with $h/r \sim 0.03$.

Recent work by Ricarte et al. (2023) measured equilibrium spin in radiative MAD simulations but focused on thicker disks, with a minimum⁷ $h/r \sim 0.18$. Direct comparison is difficult since our radiative simulations do not overlap in Eddington ratio, λ_{Edd} , space. However, for $h/r \sim 0.18$, they report a higher equilibrium spin ($a_{\text{eq}} \sim 0.8$) than what we find for $h/r = 0.1$ ($a_{\text{eq}} \sim 0.3$). Within our model, we expect $0.07 \leq a_{\text{eq}} \leq 0.3$ for such disks, in tension with their results.

Ricarte et al. (2023) also propose a general spin-down model applicable to all Eddington ratios, which we can compare to our radiative simulations at $\lambda_{\text{Edd}} = 0.35$ which have $h/r = 0.03$ (Liska et al. 2022). At this Eddington ratio they report an equilibrium spin of $a_{\text{eq}} \sim 1$, whereas we find $a_{\text{eq}} \sim 0.3$. Moreover, their results show no sign of convergence in a_{eq} for thinner disks; instead, their equilibrium spin continues increasing as disk thickness decreases, eventually reaching values consistent with the NT disk ($a_{\text{eq}} = 1$).

4.3. Observational implications

This work is timely for understanding BH spin measurements in binaries, where mass transfer—the process by which a donor star loses mass to a BH—is a key aspect of evolution and may also govern the BH spin evolution. Stellar-mass BH spins are directly measured via gravitational waves (GW) in binary mergers (Abbott et al. 2019; Wysocki et al. 2019; LIGO Scientific Collaboration et al. 2023; Edelman et al. 2023) and constrained in XRBs using X-ray reflection (Liu et al. 2008; Draghis et al. 2024). However, these methods yield conflicting spin distributions: GW observations show a distribution centered around $|a| \sim 0.2$, whereas EM observations find a distribution skewed toward higher BH spins, $a \gtrsim 0.5$. This discrepancy may arise from GW sources and XRBs belonging to distinct binary populations, which have different mass transfer histories (Gallegos-Garcia et al. 2022; Fishbach & Kalogera 2022). Spin evolution during mass transfer involves violent accretion episodes that can significantly alter the BH natal spin (Qin et al. 2022). Whether these hypercritical accretion phases are linked to ultraluminous X-ray sources (ULXs) remains uncertain, but the mere fact that ULXs exist, confirms that some binaries accrete far above Eddington (King et al. 2023). However, binary evolution studies typically assume the NT accretion disk model for spin evolution, which does not apply to disks with large-scale vertical magnetic fields. Our MAD spin-down model could yield significantly different spin distributions compared to NT models, making it a valuable case study for spin evolution in binary evolution codes.

A leading model for long GRBs is the collapsar scenario, where a rapidly rotating massive star collapses into a BH,

⁶ Difference in φ -resolution between low- and high- resolution simulation might also affect the equilibrium spin.

⁷ We note that our measurements of h/r are not entirely comparable, as they use radiative and thermal pressure to measure h/r .

launching powerful jets that produce gamma-ray emission (Woosley 1993). Our previous work on thick MADs (Lowell et al. 2024) applied to collapsar GRBs demonstrated that their high accretion rates and strong jets make them ideal systems for BH spin-down (Jacquemin-Ide et al. 2024a; Wu et al. 2024). We showed that collapsars can spin down to $a_{\text{eq}} = 0.07$ within seconds, well before the GRB ends. However, this work did not account for neutrino cooling (Chevalier 1989), which alters disk thickness and, consequently as shown here equilibrium spin. Indeed, recent work by Issa et al. (2025) finds that under neutrino cooling, collapsars spin down to a higher equilibrium spin, $a_{\text{eq}} \simeq 0.13$, and therefore fall between our cases of $h/r = 0.1$ and $h/r = 0.3$ consistent with our results. Their equilibrium spin measurement could serve as an initial condition for BH spin, which our model—better suited for binary evolution—would then further evolve.

Jet feedback is crucial for galaxy formation and the evolution of large-scale cosmological structures like galaxy clusters. Understanding BH spin evolution in luminous quasars is essential, as BH spin changes directly impact the energy injection into the galaxy and cluster environment. Recent quasar formation simulations, which track accretion disk formation and evolution within a dynamically simulated galaxy, suggest the emergence of a superthermal, toroidally dominated disk (Hopkins et al. 2024). By interpolating the final snapshot of Hopkins et al. (2024) simulation to H-AMR, Kaaz et al. (2025) found that the central BH can accrete at trans-Eddington rates, $\lambda_{\text{Edd}} \equiv \dot{m}/\dot{m}_{\text{Edd}} \sim 5$. The disk settles into a MAD-like structure similar to the thin MADs studied here. Their simplified spin-down estimates suggest spin evolution on timescales comparable to the AGN duty cycle, ~ 10 Myr. This indicates that our results on BH spin-down are highly relevant for cosmological quasar accretion, as these systems accrete rapidly and exhibit MAD-like structures. This is especially important if one wants to also understand the implications of AGN BH spin measurements for the BH accretion and merger history (Reynolds 2021).

Observations of jetted accretion disk sources (XRBS and AGN) reveal a strong correlation between jet luminosity (L_{jet}) and accretion luminosity (\dot{m}), independent of accretor mass, and spanning a wide range of Eddington ratios (λ_{Edd}) (Serjeant et al. 1998; Corbel et al. 2003; Markoff et al. 2003; Corbel et al. 2013; Zamaninasab et al. 2014). This suggests little variation in jet efficiency, $\eta_{\text{EM}} = L_{\text{jet}}/\dot{m}c^2$, across these systems. Our results show that in MADs, η_{EM} remains independent of disk thickness for $h/r \leq 0.1$, and even when comparing thick ($h/r = 0.3$) and thin ($h/r = 0.1$) disks, jet efficiency decreases by only a factor of 2 for fixed a . The small variation, within a factor of 2, in η_{EM} for fixed BH spin across different disk properties would be hard to distinguish

observationally. This might explain the universal correlation between jet luminosity and accretion rate observed across diverse astrophysical systems and Eddington.

Our results suggest that if all jetted BHs are in the MAD state, they should spin down to low spin values, $a_{\text{eq}} \lesssim 0.3$, regardless of their Eddington ratio, given sufficient time. This has significant implications for the cosmological evolution of BHs in AGN, directly impacting cosmological BH feedback. Additionally, in binary systems, these findings are crucial for LISA and LVK science, offering a potential explanation for the observed BH spin distribution.

1 BL acknowledges support by a National Science Founda-
 2 tion Graduate Research Fellowship under Grant No. DGE-
 3 2234667. BL also acknowledges support by a Illinois Space
 4 Grant Consortium (ISGC) Graduate Fellowship supported by
 5 a National Aeronautics and Space Administration (NASA)
 6 grant awarded to the ISGC. JJ acknowledges support by the
 7 NSF AST-2009884, NASA 80NSSC21K1746 and NASA
 8 XMM-Newton 80NSSC22K0799 grants. AT acknowledges
 9 support by NASA 80NSSC22K0031, 80NSSC22K0799,
 10 80NSSC18K0565 and 80NSSC21K1746 grants, and
 11 by the NSF grants AST-2009884, AST-2107839, AST-
 12 1815304, AST-1911080, AST-2206471, AST-2407475,
 13 OAC-2031997. This work was performed in part at the Kavli
 14 Institute for Theoretical Physics (KITP) supported by grant
 15 NSF PHY-2309135. This work was performed in part at As-
 16 pen Center for Physics, which is supported by National Sci-
 17 ence Foundation grant PHY-2210452. This research used re-
 18 sources of the National Energy Research Scientific Comput-
 19 ing Center, a DOE Office of Science User Facility supported
 20 by the Office of Science of the U.S. Department of Energy
 21 under Contract No. DE-AC02-05CH11231 using NERSC
 22 allocations m4603 (award NP-ERCAP0029085) and m2401.
 23 The computations in this work were, in part, run at facilities
 24 supported by the Scientific Computing Core at the Flatiron
 25 Institute, a division of the Simons Foundation. An award
 26 of computer time was provided by the ASCR Leadership
 27 Computing Challenge (ALCC), Innovative and Novel Com-
 28 putational Impact on Theory and Experiment (INCITE), and
 29 OLCF Director’s Discretionary Allocation programs under
 30 award PHY129. This research was partially carried out using
 31 resources from Calcul Quebec (<http://www.calculquebec.ca>)
 32 and Compute Canada (<http://www.computeCanada.ca>) under
 33 RAPI xsp-772-ab (PI: Daryl Haggard). This research also
 34 used HPC and visualization resources provided by the Texas
 35 Advanced Computing Center (TACC) at The University of
 36 Texas at Austin, which contributed to our results via the
 37 LRAC allocation AST20011 (<http://www.tacc.utexas.edu>).

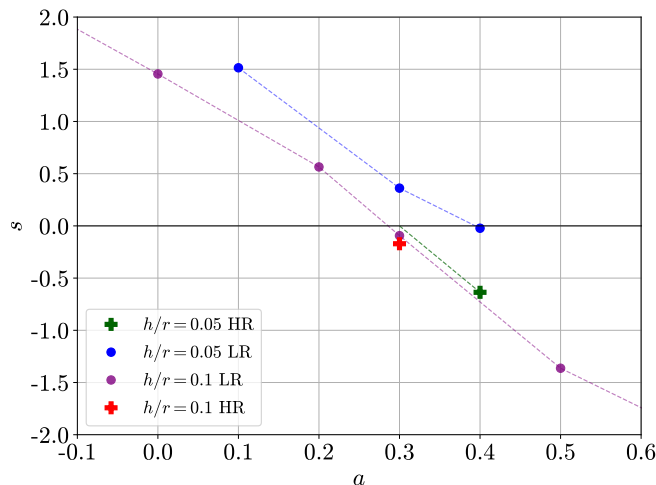


Figure 13. Convergence test for two disk scale heights of $h/r = 0.1$ and 0.05 . Purple and blue circles show low resolution (LR) simulations (give those from table). Red and green crosses show high resolution (HR) simulations run on *Summit*, with the same parameters as the LR simulations. The plot only shows results for spins between -0.1 and 0.6 to highlight the convergence near the equilibrium spins.

APPENDIX

A. CONVERGENCE TEST

We compare low- and high-resolution simulations for disk scale heights of $h/r = 0.05$ and $h/r = 0.1$. Figure 13 shows spin-up parameter values, with the primary result simulation, at standard low resolution for $h/r = 0.1$, shown in purple, yielding an equilibrium spin of 0.29 . To verify that the disk scale height is fully resolved, we ran a higher-resolution simulation on OLCF’s *Summit* (red in Figure 13). The consistency of s between resolutions confirms that lower-resolution simulations are sufficient for $h/r = 0.1$ and are therefore used for analysis in the main text.

We include lower-resolution simulations with $h/r = 0.05$ (blue) for reference, though they are not used for analysis, while the high-resolution simulation is shown in green. For a lower thermal scale height, $h/r = 0.05$, we observe significant differences in s between low-resolution simulations run on a workstation and high-resolution simulations on *Summit*. Figure 13 shows that low-resolution simulations systematically overestimate s , leading to an equilibrium spin overestimate of about 30%. Analyzing individual contributions to s (not shown) reveals that this discrepancy arises from an overestimation of hydrodynamic energy and angular momentum fluxes. We suspect that low-resolution $h/r = 0.05$ simulations fail to fully resolve the fastest-growing MRI mode, reducing turbulent dissipation, which in turn impacts these fluxes. For this reason we choose to not use the low resolution $h/r = 0.05$ for analysis in the main text.

We conclude that higher resolutions are necessary for MADs with $h/r \leq 0.05$ to accurately determine the equilibrium spin.

REFERENCES

- Abbott, B. P., Abbott, R., Abbott, T. D., et al. 2019, *The Astrophysical Journal*, 882, L24, doi: [10.3847/2041-8213/ab3800](https://doi.org/10.3847/2041-8213/ab3800)
- Avara, M. J., McKinney, J. C., & Reynolds, C. S. 2016, *Monthly Notices of the Royal Astronomical Society*, 462, 636, doi: [10.1093/mnras/stw1643](https://doi.org/10.1093/mnras/stw1643)
- Bardeen, J. M. 1970, *Nature*, 226, 64, doi: [10.1038/226064a0](https://doi.org/10.1038/226064a0)
- Batta, A., & Lee, W. H. 2014, *MNRAS*, 437, 2412, doi: [10.1093/mnras/stt2061](https://doi.org/10.1093/mnras/stt2061)
- Blandford, R. D., & Znajek, R. L. 1977, *Monthly Notices of the Royal Astronomical Society*, 179, 433, doi: [10.1093/mnras/179.3.433](https://doi.org/10.1093/mnras/179.3.433)
- Bloom, J. S., Giannios, D., Metzger, B. D., et al. 2011, *Science*, 333, 203, doi: [10.1126/science.1207150](https://doi.org/10.1126/science.1207150)
- Burrows, D. N., Kennea, J. A., Ghisellini, G., et al. 2011, *Nature*, 476, 421, doi: [10.1038/nature10374](https://doi.org/10.1038/nature10374)
- Campitiello, S., Celotti, A., Ghisellini, G., & Sbarrato, T. 2019, *Astronomy & Astrophysics*, 625, A23, doi: [10.1051/0004-6361/201834167](https://doi.org/10.1051/0004-6361/201834167)

- Chatterjee, K., & Narayan, R. 2022, *The Astrophysical Journal*, 941, 30, doi: [10.3847/1538-4357/ac9d97](https://doi.org/10.3847/1538-4357/ac9d97)
- Chen, W.-X., & Beloborodov, A. M. 2007, *ApJ*, 657, 383, doi: [10.1086/508923](https://doi.org/10.1086/508923)
- Chevalier, R. A. 1989, *The Astrophysical Journal*, 346, 847, doi: [10.1086/168066](https://doi.org/10.1086/168066)
- Chevalier, R. A. 1989, *ApJ*, 346, 847, doi: [10.1086/168066](https://doi.org/10.1086/168066)
- Corbel, S., Coriat, M., Brocksopp, C., et al. 2013, *Monthly Notices of the Royal Astronomical Society*, 428, 2500, doi: [10.1093/mnras/sts215](https://doi.org/10.1093/mnras/sts215)
- Corbel, S., Nowak, M. A., Fender, R. P., Tzioumis, A. K., & Markoff, S. 2003, *Astronomy and Astrophysics*, 400, 1007, doi: [10.1051/0004-6361:20030090](https://doi.org/10.1051/0004-6361:20030090)
- Davis, S. W., & Tchekhovskoy, A. 2020, *ARA&A*, 58, 407, doi: [10.1146/annurev-astro-081817-051905](https://doi.org/10.1146/annurev-astro-081817-051905)
- Dhang, P., Dexter, J., & Begelman, M. C. 2024, *Energy Extraction from a Black Hole by a Strongly Magnetized Thin Accretion Disk*, doi: [10.48550/arXiv.2411.02515](https://doi.org/10.48550/arXiv.2411.02515)
- Done, C., Gierliński, M., & Kubota, A. 2007, *The Astronomy and Astrophysics Review*, 15, 1, doi: [10.1007/s00159-007-0006-1](https://doi.org/10.1007/s00159-007-0006-1)
- Drachis, P. A., Miller, J. M., Costantini, E., et al. 2024, *The Astrophysical Journal*, 969, 40, doi: [10.3847/1538-4357/ad43ea](https://doi.org/10.3847/1538-4357/ad43ea)
- Edelman, B., Farr, B., & Doctor, Z. 2023, *The Astrophysical Journal*, 946, 16, doi: [10.3847/1538-4357/acb5ed](https://doi.org/10.3847/1538-4357/acb5ed)
- Esin, A. A., McClintock, J. E., & Narayan, R. 1997, *The Astrophysical Journal*, 489, 865, doi: [10.1086/304829](https://doi.org/10.1086/304829)
- Esin, A. A., Narayan, R., Cui, W., Grove, J. E., & Zhang, S.-N. 1998, *The Astrophysical Journal*, 505, 854, doi: [10.1086/306186](https://doi.org/10.1086/306186)
- Fender, R. P., Belloni, T. M., & Gallo, E. 2004, *Monthly Notices of the Royal Astronomical Society*, 355, 1105, doi: [10.1111/j.1365-2966.2004.08384.x](https://doi.org/10.1111/j.1365-2966.2004.08384.x)
- Ferreira, J., & Pelletier, G. 1995, *Astronomy and Astrophysics*, 295, 807, <http://cdsads.u-strasbg.fr/abs/1995A%26A...295..807F>
- Fishbach, M., & Kalogera, V. 2022, *The Astrophysical Journal*, 929, L26, doi: [10.3847/2041-8213/ac64a5](https://doi.org/10.3847/2041-8213/ac64a5)
- Fishbone, L. G., & Moncrief, V. 1976, *The Astrophysical Journal*, 207, 962, doi: [10.1086/154565](https://doi.org/10.1086/154565)
- Foucart, F., O'Connor, E., Roberts, L., et al. 2015, *Physical Review D*, 91, 124021, doi: [10.1103/PhysRevD.91.124021](https://doi.org/10.1103/PhysRevD.91.124021)
- Fragile, P. C., Wilson, J., & Rodriguez, M. 2012, *Monthly Notices of the Royal Astronomical Society*, 424, 524, doi: [10.1111/j.1365-2966.2012.21222.x](https://doi.org/10.1111/j.1365-2966.2012.21222.x)
- Gallegos-Garcia, M., Fishbach, M., Kalogera, V., Berry, C. P. L., & Doctor, Z. 2022, *The Astrophysical Journal Letters*, 938, L19, doi: [10.3847/2041-8213/ac96ef](https://doi.org/10.3847/2041-8213/ac96ef)
- Gammie, C. F., McKinney, J. C., & Tóth, G. 2003, *The Astrophysical Journal*, 589, 444, doi: [10.1086/374594](https://doi.org/10.1086/374594)
- Gammie, C. F., Shapiro, S. L., & McKinney, J. C. 2004, *The Astrophysical Journal*, 602, 312, doi: [10.1086/380996](https://doi.org/10.1086/380996)
- Gilfanov, M. 2010, *Lecture Notes in Physics*, Berlin Springer Verlag, 794, 17, doi: [10.1007/978-3-540-76937-8_2](https://doi.org/10.1007/978-3-540-76937-8_2)
- Goldstein, A., Connaughton, V., Briggs, M. S., & Burns, E. 2016, *The Astrophysical Journal*, 818, 18, doi: [10.3847/0004-637X/818/1/18](https://doi.org/10.3847/0004-637X/818/1/18)
- Hagen, S., & Done, C. 2023, *Estimating Black Hole Spin from AGN SED Fitting: The Impact of General-Relativistic Ray Tracing*, arXiv, doi: [10.48550/arXiv.2304.01253](https://doi.org/10.48550/arXiv.2304.01253)
- Hopkins, P. F., Squire, J., Su, K.-Y., et al. 2024, *The Open Journal of Astrophysics*, 7, 19, doi: [10.21105/astro.2310.04506](https://doi.org/10.21105/astro.2310.04506)
- Hopkins, P. F., Squire, J., Su, K.-Y., et al. 2024, *The Open Journal of Astrophysics*, 7, 19, doi: [10.21105/astro.2310.04506](https://doi.org/10.21105/astro.2310.04506)
- Igumenshchev, I. V., Narayan, R., & Abramowicz, M. A. 2003, *The Astrophysical Journal*, 592, 1042, doi: [10.1086/375769](https://doi.org/10.1086/375769)
- Inayoshi, K., Haiman, Z., & Ostriker, J. P. 2016, *Monthly Notices of the Royal Astronomical Society*, 459, 3738, doi: [10.1093/mnras/stw836](https://doi.org/10.1093/mnras/stw836)
- Issa, D., Lowell, B., Jacquemin-Ide, J., Liska, M., & Tchekhovskoy, A. 2025, *Black Hole Spin-down in Collapsars in 3D Neutrino Transport GRMHD Simulations*, doi: [10.48550/arXiv.2502.08732](https://doi.org/10.48550/arXiv.2502.08732)
- Ivezić, v., Menou, K., Knapp, G. R., et al. 2002, *The Astronomical Journal*, 124, 2364, doi: [10.1086/344069](https://doi.org/10.1086/344069)
- Jacquemin-Ide, J., Gottlieb, O., Lowell, B., & Tchekhovskoy, A. 2024a, *The Astrophysical Journal*, 961, 212, doi: [10.3847/1538-4357/ad02f0](https://doi.org/10.3847/1538-4357/ad02f0)
- Jacquemin-Ide, J., Lesur, G., & Ferreira, J. 2021, *Astronomy and Astrophysics*, 647, A192, doi: [10.1051/0004-6361/202039322](https://doi.org/10.1051/0004-6361/202039322)
- Jacquemin-Ide, J., Rincon, F., Tchekhovskoy, A., & Liska, M. 2024b, *Monthly Notices of the Royal Astronomical Society*, 532, 1522, doi: [10.1093/mnras/stae1538](https://doi.org/10.1093/mnras/stae1538)
- Jiang, Y.-F., & Blaes, O. 2020, *The Astrophysical Journal*, 900, 25, doi: [10.3847/1538-4357/aba4b7](https://doi.org/10.3847/1538-4357/aba4b7)
- Jiang, Y.-F., & Dai, L. 2024, arXiv e-prints, arXiv:2408.16856, doi: [10.48550/arXiv.2408.16856](https://doi.org/10.48550/arXiv.2408.16856)
- Kaaz, N., Liska, M., Tchekhovskoy, A., Hopkins, P. F., & Jacquemin-Ide, J. 2024, arXiv e-prints, arXiv:2410.01877, doi: [10.48550/arXiv.2410.01877](https://doi.org/10.48550/arXiv.2410.01877)
- Kaaz, N., Liska, M., Tchekhovskoy, A., Hopkins, P. F., & Jacquemin-Ide, J. 2025, *The Astrophysical Journal*, 979, 248, doi: [10.3847/1538-4357/ad9a86](https://doi.org/10.3847/1538-4357/ad9a86)
- Kellermann, K. I., Condon, J. J., Kimball, A. E., Perley, R. A., & Ivezić, v. 2016, *The Astrophysical Journal*, 831, 168, doi: [10.3847/0004-637X/831/2/168](https://doi.org/10.3847/0004-637X/831/2/168)
- Kellermann, K. I., Sramek, R., Schmidt, M., Shaffer, D. B., & Green, R. 1989, *The Astronomical Journal*, 98, 1195, doi: [10.1086/115207](https://doi.org/10.1086/115207)
- King, A., Lasota, J.-P., & Middleton, M. 2023, *New Astronomy Reviews*, 96, 101672, doi: [10.1016/j.newar.2022.101672](https://doi.org/10.1016/j.newar.2022.101672)

- Komissarov, S. S. 1999, *MNRAS*, 308, 1069, doi: [10.1046/j.1365-8711.1999.02783.x](https://doi.org/10.1046/j.1365-8711.1999.02783.x)
- Kong, M., & Ho, L. C. 2018, *The Astrophysical Journal*, 859, 116, doi: [10.3847/1538-4357/aabe2a](https://doi.org/10.3847/1538-4357/aabe2a)
- LIGO Scientific Collaboration, and KAGRA Collaboration, V. C., Abbott, R., Abbott, T., et al. 2023, *Physical Review X*, 13, 011048, doi: [10.1103/PhysRevX.13.011048](https://doi.org/10.1103/PhysRevX.13.011048)
- Liska, M., Hesp, C., Tchekhovskoy, A., et al. 2018, *Monthly Notices of the Royal Astronomical Society*, 474, L81, doi: [10.1093/mnras/slx174](https://doi.org/10.1093/mnras/slx174)
- Liska, M., Tchekhovskoy, A., Ingram, A., & van der Klis, M. 2019, *Monthly Notices of the Royal Astronomical Society*, 487, 550, doi: [10.1093/mnras/stz834](https://doi.org/10.1093/mnras/stz834)
- Liska, M., Tchekhovskoy, A., & Quataert, E. 2020, *Monthly Notices of the Royal Astronomical Society*, 494, 3656, doi: [10.1093/mnras/staa955](https://doi.org/10.1093/mnras/staa955)
- Liska, M. T. P., Musoke, G., Tchekhovskoy, A., Porth, O., & Beloborodov, A. M. 2022, *The Astrophysical Journal Letters*, 935, L1, doi: [10.3847/2041-8213/ac84db](https://doi.org/10.3847/2041-8213/ac84db)
- Liska, M. T. P., Chatterjee, K., Issa, D., et al. 2022, *ApJS*, 263, 26, doi: [10.3847/1538-4365/ac9966](https://doi.org/10.3847/1538-4365/ac9966)
- Liu, J., McClintock, J. E., Narayan, R., Davis, S. W., & Orosz, J. A. 2008, *The Astrophysical Journal*, 679, L37, doi: [10.1086/588840](https://doi.org/10.1086/588840)
- Lowell, B., Jacquemin-Ide, J., Tchekhovskoy, A., & Duncan, A. 2024, *The Astrophysical Journal*, 960, 82, doi: [10.3847/1538-4357/ad09af](https://doi.org/10.3847/1538-4357/ad09af)
- Lubow, S. H., & Spruit, H. C. 1995, *The Astrophysical Journal*, 445, 337, doi: [10.1086/175698](https://doi.org/10.1086/175698)
- Manikantan, V., Kaaz, N., Jacquemin-Ide, J., et al. 2024, *ApJ*, 965, 175, doi: [10.3847/1538-4357/ad323d](https://doi.org/10.3847/1538-4357/ad323d)
- Marcel, G., Ferreira, J., Petrucci, P.-O., et al. 2018, *Astronomy and Astrophysics*, 617, A46, doi: [10.1051/0004-6361/201833124](https://doi.org/10.1051/0004-6361/201833124)
- Marcel, G., Ferreira, J., Clavel, M., et al. 2019, *Astronomy & Astrophysics*, 626, A115, doi: [10.1051/0004-6361/201935060](https://doi.org/10.1051/0004-6361/201935060)
- Markoff, S., Nowak, M., Corbel, S., Fender, R., & Falcke, H. 2003, *Astronomy and Astrophysics*, 397, 645, doi: [10.1051/0004-6361:20021497](https://doi.org/10.1051/0004-6361:20021497)
- Metzger, B. D. 2019, *Living Reviews in Relativity*, 23, 1, doi: [10.1007/s41114-019-0024-0](https://doi.org/10.1007/s41114-019-0024-0)
- Miller-Jones, J. C. A., Bahramian, A., Orosz, J. A., et al. 2021, *Science*, 371, 1046, doi: [10.1126/science.abb3363](https://doi.org/10.1126/science.abb3363)
- Mitsuda, K., Inoue, H., Koyama, K., et al. 1984, *Publications of the Astronomical Society of Japan*, 36, 741, <https://ui.adsabs.harvard.edu/abs/1984PASJ...36..741M>
- Moderski, R., & Sikora, M. 1996, *Monthly Notices of the Royal Astronomical Society*, 283, 854, doi: [10.1093/mnras/283.3.854](https://doi.org/10.1093/mnras/283.3.854)
- Nakar, E. 2020, *Physics Reports*, 886, 1, doi: [10.1016/j.physrep.2020.08.008](https://doi.org/10.1016/j.physrep.2020.08.008)
- Narayan, R., Chael, A., Chatterjee, K., Ricarte, A., & Curd, B. 2022, *Monthly Notices of the Royal Astronomical Society*, 511, 3795, doi: [10.1093/mnras/stac285](https://doi.org/10.1093/mnras/stac285)
- Narayan, R., & Yi, I. 1994, *ApJL*, 428, L13, doi: [10.1086/187381](https://doi.org/10.1086/187381)
- . 1995a, *ApJ*, 444, 231, doi: [10.1086/175599](https://doi.org/10.1086/175599)
- . 1995b, *ApJ*, 452, 710, doi: [10.1086/176343](https://doi.org/10.1086/176343)
- Noble, S. C., Gammie, C. F., McKinney, J. C., & Del Zanna, L. 2006, *The Astrophysical Journal*, 641, 626, doi: [10.1086/500349](https://doi.org/10.1086/500349)
- Noble, S. C., Krolik, J. H., & Hawley, J. F. 2009, *The Astrophysical Journal*, 692, 411, doi: [10.1088/0004-637X/692/1/411](https://doi.org/10.1088/0004-637X/692/1/411)
- Novikov, I. D., & Thorne, K. S. 1973, *Astrophysics of black holes*, <https://ui.adsabs.harvard.edu/abs/1973blho.conf..343N>
- Paczynski, B., & Xu, G. 1994, *ApJ*, 427, 708, doi: [10.1086/174178](https://doi.org/10.1086/174178)
- Penrose, R. 1969, *Nuovo Cimento Rivista Serie*, 1, 252, <https://ui.adsabs.harvard.edu/abs/1969NCimR...1..252P>
- Popham, R., Woosley, S. E., & Fryer, C. 1999, *The Astrophysical Journal*, 518, 356, doi: [10.1086/307259](https://doi.org/10.1086/307259)
- Pringle, J. E., & Rees, M. J. 1972, *Astronomy and Astrophysics*, 21, 1, <https://ui.adsabs.harvard.edu/abs/1972A&A....21....1P>
- Qiao, E., & Liu, B. F. 2012, *The Astrophysical Journal*, 744, 145, doi: [10.1088/0004-637X/744/2/145](https://doi.org/10.1088/0004-637X/744/2/145)
- . 2013, *The Astrophysical Journal*, 764, 2, doi: [10.1088/0004-637X/764/1/2](https://doi.org/10.1088/0004-637X/764/1/2)
- Qin, Y., Shu, X., Yi, S., & Wang, Y.-Z. 2022, *Research in Astronomy and Astrophysics*, 22, 035023, doi: [10.1088/1674-4527/ac4ca4](https://doi.org/10.1088/1674-4527/ac4ca4)
- Remillard, R. A., & McClintock, J. E. 2006, *Annual Review of Astronomy and Astrophysics*, 44, 49, doi: [10.1146/annurev.astro.44.051905.092532](https://doi.org/10.1146/annurev.astro.44.051905.092532)
- Reynolds, C. S. 2021, *Annual Review of Astronomy and Astrophysics*, 59, 117, doi: [10.1146/annurev-astro-112420-035022](https://doi.org/10.1146/annurev-astro-112420-035022)
- Ricarte, A., Narayan, R., & Curd, B. 2023, *Recipes for Jet Feedback and Spin Evolution of Black Holes with Strongly-Magnetized Super-Eddington Accretion Disks*, arXiv, doi: [10.48550/arXiv.2307.04621](https://doi.org/10.48550/arXiv.2307.04621)
- Salvesen, G., Simon, J. B., Armitage, P. J., & Begelman, M. C. 2016, *Monthly Notices of the Royal Astronomical Society*, 457, 857, doi: [10.1093/mnras/stw029](https://doi.org/10.1093/mnras/stw029)
- Scepi, N., Begelman, M. C., & Dexter, J. 2023, *Magnetic support, wind-driven accretion, coronal heating, and fast outflows in a thin magnetically arrested disc*, arXiv, doi: [10.48550/arXiv.2302.10226](https://doi.org/10.48550/arXiv.2302.10226)
- Serjeant, S., Rawlings, S., Lacy, M., et al. 1998, *Monthly Notices of the Royal Astronomical Society*, 294, 494, doi: [10.1046/j.1365-8711.1998.01303.x](https://doi.org/10.1046/j.1365-8711.1998.01303.x)
- Shakura, N. I., & Sunyaev, R. A. 1973a, *Astronomy and Astrophysics*, 24, 337, <https://ui.adsabs.harvard.edu/abs/1973A&A....24..337S>

- . 1973b, *Astronomy and Astrophysics*, 24, 337.
<https://ui.adsabs.harvard.edu/abs/1973A&A....24..337S>
- . 1976, *Monthly Notices of the Royal Astronomical Society*, 175, 613, doi: [10.1093/mnras/175.3.613](https://doi.org/10.1093/mnras/175.3.613)
- Shapiro, S. L., & Teukolsky, S. A. 1983, Black holes, white dwarfs and neutron stars. The physics of compact objects, doi: [10.1002/9783527617661](https://doi.org/10.1002/9783527617661)
- Siegel, D. M., Barnes, J., & Metzger, B. D. 2019, *Nature*, 569, 241, doi: [10.1038/s41586-019-1136-0](https://doi.org/10.1038/s41586-019-1136-0)
- Singh, C. B., Garofalo, D., & Lang, B. 2021, *Galaxies*, 9, 10, doi: [10.3390/galaxies9010010](https://doi.org/10.3390/galaxies9010010)
- Squire, J., Quataert, E., & Hopkins, P. F. 2024, arXiv e-prints, arXiv:2409.05467, doi: [10.48550/arXiv.2409.05467](https://doi.org/10.48550/arXiv.2409.05467)
- Squire, J., Quataert, E., & Hopkins, P. F. 2024, Rapid, strongly magnetized accretion in the zero-net-vertical-flux shearing box, doi: [10.48550/arXiv.2409.05467](https://doi.org/10.48550/arXiv.2409.05467)
- Sądowski, A., & Narayan, R. 2015a, *Monthly Notices of the Royal Astronomical Society*, 454, 2372, doi: [10.1093/mnras/stv2022](https://doi.org/10.1093/mnras/stv2022)
- . 2015b, *Monthly Notices of the Royal Astronomical Society*, 453, 3213, doi: [10.1093/mnras/stv1802](https://doi.org/10.1093/mnras/stv1802)
- Sądowski, A., Narayan, R., Tchekhovskoy, A., & Zhu, Y. 2013, *Monthly Notices of the Royal Astronomical Society*, 429, 3533, doi: [10.1093/mnras/sts632](https://doi.org/10.1093/mnras/sts632)
- Sądowski, A., Wielgus, M., Narayan, R., et al. 2017, *Monthly Notices of the Royal Astronomical Society*, 466, 705, doi: [10.1093/mnras/stw3116](https://doi.org/10.1093/mnras/stw3116)
- Tchekhovskoy, A. 2015, in *Astrophysics and Space Science Library*, Vol. 414, The Formation and Disruption of Black Hole Jets, ed. I. Contopoulos, D. Gabuzda, & N. Kylafis, 45, doi: [10.1007/978-3-319-10356-3_3](https://doi.org/10.1007/978-3-319-10356-3_3)
- Tchekhovskoy, A. 2019, HARMPI: 3D massively parallel general relativistic MHD code, *Astrophysics Source Code Library*, record ascl:1912.014
- Tchekhovskoy, A., & Giannios, D. 2015, *MNRAS*, 447, 327, doi: [10.1093/mnras/stu2229](https://doi.org/10.1093/mnras/stu2229)
- Tchekhovskoy, A., McKinney, J. C., & Narayan, R. 2008, *Monthly Notices of the Royal Astronomical Society*, 388, 551, doi: [10.1111/j.1365-2966.2008.13425.x](https://doi.org/10.1111/j.1365-2966.2008.13425.x)
- Tchekhovskoy, A., McKinney, J. C., & Narayan, R. 2012, in *Journal of Physics Conference Series*, Vol. 372, *Journal of Physics Conference Series (IOP)*, 012040, doi: [10.1088/1742-6596/372/1/012040](https://doi.org/10.1088/1742-6596/372/1/012040)
- Tchekhovskoy, A., Metzger, B. D., Giannios, D., & Kelley, L. Z. 2014, *Monthly Notices of the Royal Astronomical Society*, 437, 2744, doi: [10.1093/mnras/stt2085](https://doi.org/10.1093/mnras/stt2085)
- Tchekhovskoy, A., Narayan, R., & McKinney, J. C. 2010, *The Astrophysical Journal*, 711, 50, doi: [10.1088/0004-637X/711/1/50](https://doi.org/10.1088/0004-637X/711/1/50)
- Tchekhovskoy, A., Narayan, R., & McKinney, J. C. 2011, *MNRAS*, 418, L79, doi: [10.1111/j.1745-3933.2011.01147.x](https://doi.org/10.1111/j.1745-3933.2011.01147.x)
- Woosley, S. E. 1993, *The Astrophysical Journal*, 405, 273, doi: [10.1086/172359](https://doi.org/10.1086/172359)
- Wu, Z.-F., Damoulakis, M., Beniamini, P., & Giannios, D. 2024, Maximal Jet Energy of Gamma-Ray Bursts through the Blandford-Znajek Mechanism, doi: [10.48550/arXiv.2411.12850](https://doi.org/10.48550/arXiv.2411.12850)
- Wytke, J. S. B., & Loeb, A. 2012, *Monthly Notices of the Royal Astronomical Society*, 425, 2892, doi: [10.1111/j.1365-2966.2012.21127.x](https://doi.org/10.1111/j.1365-2966.2012.21127.x)
- Wysocki, D., Lange, J., & O’Shaughnessy, R. 2019, *Physical Review D*, 100, 043012, doi: [10.1103/PhysRevD.100.043012](https://doi.org/10.1103/PhysRevD.100.043012)
- Yuan, F., & Narayan, R. 2014, *ARA&A*, 52, 529, doi: [10.1146/annurev-astro-082812-141003](https://doi.org/10.1146/annurev-astro-082812-141003)
- Zamaninasab, M., Clausen-Brown, E., Savolainen, T., & Tchekhovskoy, A. 2014, *Nature*, 510, 126, doi: [10.1038/nature13399](https://doi.org/10.1038/nature13399)
- Zimniak, N., Ferreira, J., & Jacquemin-Ide, J. 2024, *Astronomy and Astrophysics*, 692, A99, doi: [10.1051/0004-6361/202450501](https://doi.org/10.1051/0004-6361/202450501)